UPPSALA
UNIVERSITET

Digital Comprehensive Summaries of Uppsala Dissertations from the Faculty of Science and Technology 2195

Seismic Exploration Solutions for Deep-Targeting Metallic Mineral Deposits

From high-fold 2D to sparse 3D, and deep-learning workflows

MAGDALENA MARKOVIC

ACTA
UNIVERSITATIS
UPSALIENSIS
UPPSALA
2022

ISSN 1651-6214
ISBN 978-91-513-1603-1
URN urn:nbn:se:uu:diva-481754

Dissertation presented at Uppsala University to be publicly examined in Hambergsalen, Geocentrum, Villavägen 16, Uppsala, Friday, 11 November 2022 at 10:00 for the degree of Doctor of Philosophy. The examination will be conducted in English. Faculty examiner: Dr. Gilles Bellefleur (Geological Survey of Canada).

Abstract
Markovic, M. 2022. Seismic Exploration Solutions for Deep-Targeting Metallic Mineral Deposits. From high-fold 2D to sparse 3D, and deep-learning workflows. *Digital Comprehensive Summaries of Uppsala Dissertations from the Faculty of Science and Technology* 2195. 82 pp. Uppsala: Acta Universitatis Upsaliensis. ISBN 978-91-513-1603-1.

Mineral exploration has in recent years moved its focus to greater depths than ever before, particularly in brown fields. Exploring new deposits at depth, if economical, would not only expand the life of mine but also provide minimal environmental impacts. It allows the existing mining infrastructures to be used for a longer period. Exploration at depth, however, is challenging and requires a multidisciplinary team and methods, and innovative thinking for generating new targets and effective exploration expenditure. The application of seismic methods for mineral exploration has increasingly been conducted over the past 20 years because they provide high-resolution subsurface images, and retain good resolution with depth as compared with other geophysical methods. Nevertheless, and despite challenges in hardrock settings, only limited attention has been given to seismic interpretations, often performed subjectively. With the growing application of machine-learning solutions, hardrock seismic data can benefit these for improved interpretations and target generations.

This thesis showcases different workflows developed for deep-targeting metallic mineral deposits, starting from high-fold 2D, through sparse 3D reflection imaging and the implementation of deep-learning algorithms for diffraction pattern recognitions. Three different deposits were studied from Sweden and Canada. The Blötberget iron-oxide mineralization in central Sweden was first targeted in 2D, followed-up, a sparse 3D dataset was acquired enabling to image the mineralization both laterally and with depth, providing good knowledge on subsurface structures controlling the geometry of the deposits. In Canada, Halfmile Lake and Matagami mining sites were studied due to the accessibility to 3D seismic datasets, which contained diffraction signals as deposit responses. Deeplearning algorithms were utilized for the proof-of-concept and at the same time helped to generate new potential targets from other diffraction signals that were not obvious to an interpreter's eye due to their incomplete tails originated outside of the seismic volume. The studies in this thesis show the effectiveness of seismic methods for mineral exploration at depth, especially in 3D, as they provide, among others, structural interpretation for future mineplanning purposes. Deep-learning solutions provide improved results for diffraction delineation and denoising and have great potential for hardrock seismics.

Keywords: Exploration, Seismic, Mineral Deposits, Diffraction, Deep learning

Magdalena Markovic, Department of Earth Sciences, Geophysics, Villav. 16, Uppsala University, SE-75236 Uppsala, Sweden.

ISSN 1651-6214
ISBN 978-91-513-1603-1
URN urn:nbn:se:uu:diva-481754 (http://urn.kb.se/resolve?urn=urn:nbn:se:uu:diva-481754)

To my mother Vesna, father Zoran
and Serbian homeland

Supervisor
Professor Alireza Malehmir
Department of Earth Sciences – Geophysics Program
Uppsala University, Sweden

Co-supervisor
Associate Professor Ayse Kaslilar Sisman
Department of Earth Sciences – Geophysics Program
Uppsala University, Sweden

Faculty opponent
Dr. Gilles Bellefleur
Natural Resources Canada
Geological Survey of Canada

Committee members
Dr. Suvi Heinonen
Unit for Geophysical Solutions
Geological Survey of Finland

Dr. Tijmen Jan Moser
Geophysical Advisor
Moser Geophysical Services, The Netherlands

Associate Professor Ivan Vasconcelos
Department of Earth Sciences
Utrecht University, The Netherlands

Dr. Maria Ask (reserve)
Department of Earth Sciences – Geophysics Program
Uppsala University, Sweden

List of Papers

This thesis is based on the following papers, which are referred to in the text by their Roman numerals.

I. **Markovic M.**, Maries G., Malehmir, A., von Ketelholdt, J., Backström, E., Schon M., and Marsden, P. (2020) Deep reflection seismic imaging of iron-oxide deposits in the Ludvika mining area of central Sweden. *Geophysical Prospecting* 68: 7–23.

II. Malehmir, A., **Markovic, M.**, Marsden, P., Gil, A., Buske, S., Sito, L., Bäckström, E., Sadeghi, M., and Luth, S. (2021) Sparse 3D reflection seismic survey for deep-targeting iron oxide deposits and their host rocks, Ludvika Mines, Sweden. *Solid Earth* 12: 483–502.

III. **Markovic, M.**, Malehmir, R., and Malehmir, A. (2022a) Diffraction pattern recognition using deep semantic segmentation. *Near Surface Geophysics*, 20(5), 507-518.

IV. **Markovic, M.**, Malehmir, R., and Malehmir, A. (2022b) Diffraction denoising using unsupervised learning technique. In revision in *Geophysical Prospecting*.

Reprints were made with permission from the respective publishers.

Additionally, during my PhD, I have contributed to the following papers, which are not included in this thesis:

Markovic M., Maries G., Malehmir, A., Bäckström, E., Schon M., Jakobsson, J., and Marsden, P. (2018) Deep targeting iron-oxide mineralization using reflection seismic method: a case study from the Ludvika mines of Sweden. In *2nd Conference on Geophysics for Mineral Exploration and Mining*. Extended abstract.

Markovic M., Malehmir, A., Socco, V., Holmes, P. (2019) Young Professional Aspects of the Smart Exploration Project: Career Management, Marketing and Sustainability. In *81st EAGE Conference and Exhibition 2019*. Extended abstract.

Malehmir, A., Donoso, G., **Markovic M.**, Maries, G., Dynesius, L., Brodic, B., Pecheco, N., Marsden, P., Bäckström, E., Penney, M., and Araujo, V. (2019) Smart Exploration: from legacy data to state-of-the-art data acquisition and imaging. *First break* 37(8): 71–74.

Markovic, M., Malehmir, A., Buske, S., Bäckström, E., and Marsden, P. (2020) Sparse 3D Reflection Seismic Survey at Ludvika Mines of South-Central Sweden. In *3rd Conference on Geophysics for Mineral Exploration and Mining*. Extended abstract.

Hloušek, F., Malinowski, M., Buske, S., Bräunig, L., Singh, B., Malehmir, A., **Markovic, M.**, Koivisto, E., Heinonen, S., Sito, L., Juurela, S., Bäckström, E., Schön, M., and Marsden, P. (2020) A tailored workflow for advanced high-resolution seismic imaging of mineral exploration targets. In *Mineral Exploration Symposium*. Extended abstract.

Malehmir, A., **Markovic, M.**, Marsden, P., Buske, S., Dito, L., and Backström, E. (2020) Advancing Reflection Seismic Methods for Deep-Targeting Mineral Deposits: A Series of 2D and 3D Surveys. In *82nd EAGE Conference and Exhibition 2020*. Extended abstract.

Markovic, M., Malehmir, R., and Malehmir, A. (2021) Diffraction Recognition Using Deep Learning. In *2nd Conference on Geophysics for Infrastructure Planning, Monitoring and BIM*. Extended abstract.

Hloušek, F., Malinowski, M., Bräunig, L., Buske, S., Malehmir, A., **Markovic, M.**, Sito, L., Marsden, P., and Bäckström, E. (2022) 3D reflection seismic imaging of the iron-oxide deposits in the Ludvika mining area (Sweden) using a focusing pre-stack depth migration approach. *Solid Earth* 13 (5): 917–934.

Markovic, M., Malehmir, R., and Malehmir, A. (2022) Diffraction Denoising Using Autoencoder. In *83rd EAGE Conference and Exhibition 2020*. Extended abstract.

Markovic, M., Malehmir, A., and Malehmir, R. (2022) Coupled Hough-transform and deep learning for improved diffraction delineation. In *4th Conference on Geophysics for Mineral Exploration and Mining*. Extended abstract.

Kaslilar, A., Wilczyński, Z., **Markovic, M.**, Marsden, P., Manzi, M., and Malehmir, A. (2022) A prefeasibility study for passive seismic imaging in hard rock environment. In *4th Conference on Geophysics for Mineral Exploration and Mining*. Extended abstract.

Contributions

Paper I: I processed the two seismic data sets prepared by A. Malehmir and G. Maries in 2015 and 2016, respectively. The initial manuscript was written by me and G. Maries., and J. von Ketelholdt helped with the implementation of the curvelet denoising algorithm. A. Malehmir, M. Schön, E. Bäckström and P. Marsden provided valuable input for the data processing and interpretation. All authors improved the manuscript through several iterations.

Paper II: I participated in the design of the sparse 3D seismic survey and partly took part in the data acquisition. I prepared all the data for processing. A. Malehmir processed the data and together we discussed the results and data interpretation. A. Malehmir wrote the initial manuscript and all authors contributed to its final version.

Paper III: I prepared scripts from SEG-Y to image conversion and generated synthetic seismic sections for the training. R. Malehmir provided the deep-learning algorithm, which we together developed for the case studies. Together with A. Malehmir we scripted diffraction traveltime modelling in 3D. I wrote the initial manuscript and R. Malehmir, and A. Malehmir provided their suggestions for the final version of the manuscript.

Paper IV: The deep-learning algorithm was provided by R. Malehmir and with him I developed the algorithm for the case studies. I generated additional synthetic sections to improve the training model. Together with A. Malehmir we scripted a workflow for the application of the Hough transform in the deep-learning solution. I wrote the initial manuscript, and A. Malehmir and R. Malehmir provided their suggestions in a few iterations until its final version.

Contents

Abbreviations

2D	Two-dimensional
3D	Three-dimensional
3C	Three-component
CDP	Common Depthpoint
CMP	Common Midpoint
CNN	Convolutional Neural Network
DAS	Distributed Acoustic Sensing
DMO	Dip Moveout
EU	European Union
FDCT	Fast Discrete Curvelet Transform
Ga	Billion years ago
GPR	Ground Penetrating Radar
Hz	Hertz
kg	Kilogram
km	Kilometer
LMO	Linear Moveout
m	Meter
Ma	Million years ago
MEMS	Micro Electro-Mechanical System
ms	Millisecond
Mt	Megaton
NMO	Normal Moveout
NW	Northwest
R&D	Research and Development
RMS	Root Mean Square
s	Second
SE	Southeast
SEG-Y	Society of Exploration Geophysicists – revision Y
UAV	Unmanned Aerial Vehicle
VMS	Volcanogenic Massive Sulphide

1 Introduction

Raw materials are a vital part of everyday life. They provide basic essentials for our well-being and effective functioning. With technological developments, the need for exploring and exploiting new resources has increased. However, opening a new mine can sometimes have a large impact on environment, hence current exploration trends are focused on exploring new deposits at greater depths near existing mines (brownfields and in-mine) or where infrastructures are in place. Potential field methods are standardly used for mineral exploration, yet they are constrained by decrement of resolution with depth and their inherent modeling ambiguity or non-uniqueness. However, other advancements in sensor and drone technologies have led to improved, for example, UAV-based potential methods, such as magnetic surveys for high-resolution and effective surveying. They can also assist fast planning of other types of surveys (Malehmir et al., 2017a). For deep-targeting mineral deposits, reflection seismic methods have a great advantage. They retain a good resolution with depth and provide robust imaging results if carefully planned, acquired, and interpreted considering complexity of the geology being addressed. Originally developed for oil and gas industry, the method has now routinely been adapted for hardrock and crystalline rock settings (e.g., Milkereit et al., 1996; Bellefleur et al., 2004; Dehghannejad et al., 2010; Cheraghi et al., 2012; Koivisto et al., 2012; Malehmir et al., 2012, 2014; Manzi et al., 2012; Urosevic et al., 2013; Place et al., 2015; Heinonen et al., 2019).

Given sometimes their criticality for the industry and improved living standards, several R&D programme worldwide and particularly within the EU have been initiated calling for innovative and effective solutions for sustainable exploration and exploitation of raw materials. This thesis work was performed within one of as such, the Smart Exploration™ project, sponsored by the European Commission under the Horizon 2020 grant program. The project itself included partners from both research and industry background for developing novel technologies and solutions for mineral exploration. The project benefited from five exploration sites, among which Ludvika Mines in Sweden was given the highest focus for both technological testing but also for methodological workflows. Nearly half of this PhD thesis work dealt with the Ludvika Mine site and the remaining half with data from two sites in Canada. In all these cases, a goal was to generate added value for the mining companies

involved to maximize the value of the developed solutions while testing and developing ideas for data acquisition and processing as well as interpretation through state-of-the-art solutions.

1.1 Motivation and objectives

The first study site covered in this thesis is located at the historical Blötberget mine, which was exploiting iron-oxide deposits for several decades. The site itself is unique in terms of numbers of studies conducted to validate state-of-the-art field instruments and to developed new and adapt conventional seismic data processing workflows for deep-targeting of iron-oxide deposits. The first-ever seismic survey at this site was carried out in 2015 (Malehmir et al., 2017b) with the purpose of testing a MEMS-based landstreamer system (Brodic et al., 2015) in combination with conventional plant-type geophones for mineral exploration of medium (<500-800 m) target depths. It was tested for its cost-effective, time and budget-wise, idea. The results obtained from this survey showed a great potential to further employ reflection seismic methods at the site since the iron-oxide mineralization showed strong contrast compared to the volcano-sedimentary host rocks. Another follow-up survey was carried out in 2016, where the data were collected conventionally with plant type 10 Hz geophones, along the same profile but using a higher fold and fixed geometry. Additional perpendicular profile was deployed to study lateral extension of the mineralization (Maries et al., 2020). The 2016 profile alone was the subject of several studies for seismic processing and imaging workflow developments such surface-wave attenuation using seismic interferometry and curvelet transforms (Balestrini et al., 2020; Markovic et al., 2020; **Paper I**); adapting pre-stack depth migration and reverse time migration algorithms (Bräunig et al., 2020; Ding and Malehmir, 2021); improved static corrections with surface wave analysis (Papadopoulou et al., 2020); all conducted within the frame of the Smart Exploration™ project.

Paper I of this thesis focused on developing a workflow and how-to solution for obtaining even a higher fold 2D data by merging the data collected in the 2015 and 2016 field campaigns. The above-mentioned studies were the base for planning a sparse 3D survey in 2019 (**Paper II)**, where one of the profiles overlapped with the position of the 2D profile of **Paper I**. The 3D survey, reported for the first time in Sweden for the purpose of mineral exploration (Malehmir et al., 2021; **Paper II)** employed industry-standard seismic processing workflows, however, the same dataset was used to study pre-stack depth migration algorithms (Hloušek et al., 2022) and full-waveform inversion and reverse time migration (Singh et al., 2022). Several other surveys at the same position of the 2D profile were conducted for validation of broadband seismic source (Pertuz et al., 2022), and most recently passive- and active-source surface and downhole DAS, broadband surface array and 10-Hz

3C recordings (Kaslilar et al., 2022; Malehmir, 2022). Much of the focus of **Paper II** was on the planning of the survey and showcasing that a 3D survey even sparse can add much greater information than 2D surveys. As a regular 3D survey meant excessive forest cuttings and footprints, much of the research focused on obtain a uniform fold 3D dataset taking advantage of existing forest roads. As a side benefit, the study also aimed to motivate mining companies to embrace 3D seismic methods in Sweden for deep exploration purposes hence it should be considered a pioneer work opening new frontiers for 3D surveys inside Sweden.

In **Papers III** and **IV**, the main motivation was to study diffraction response of mineral deposits in hardrock seismic data; it was triggered from the observation of several weak diffraction on the 3D dataset from Ludvika. They were interpreted to be associated with possible faulting of the mineralization. The initial idea was to employ deep-learning algorithms for diffraction pattern recognition on the inlines from the dataset shown in **Paper II**, like those of diffraction delineation in sedimentary settings (e.g., Dell et al., 2020; Tschannen et al., 2020; Lowney et al., 2021; Bauer et al., 2022). Given the weak diffraction response and limited number of training images (inlines) and complex nature of the 3D dataset (sparsity), it was not possible to obtain a training model, which could delineate the diffraction. Therefore, the developed deep-learning algorithms were tested on other 3D datasets from Canada to showcase their effectiveness because these datasets contained strong diffraction response originated from known VMS deposits.

In **Paper III**, a 3D hardrock seismic dataset collected at the Halfmile Lake site in the Bathurst Mining Camp in Canada was used for testing the U-net algorithm for diffraction pattern recognition on inlines from the seismic cube reprocessed by Malehmir and Bellefleur (2009). Besides completely recognizing a diffraction response of the known VMS deposit (deep zone), the algorithm provided additional delineation of a never trained for and never noted in earlier studies incomplete diffraction signal at the edge of the seismic cube. Assuming a tip diffraction, it was possible to 3D model and estimate the spatial origin of the diffraction. Given its strong amplitude, the diffraction signal might have a similar origin as the known deep zone VMS deposit.

In **Paper IV,** the autoencoder algorithm was used for diffraction denoising and delineation of another VMS deposit in Canada, Bell Allard, at the Matagami mining district. As the autoencoder is an unsupervised deep-learning algorithm and may suffer depending on the quality of the data, additional image processing workflows were implemented to help delineation of the diffraction signal but this time on timeslice where it was simpler to target the circular nature of the diffraction compared to the inlines or crosslines where diffraction tails and steep reflections showed better temporal-spatial coherency and difficult for the autoencoder to provide a suitable unsupervised training dataset.

This thesis showcases different methodologies for deep-targeting of iron-oxide and VMS deposits and target generations, has the following objectives:

(1) Providing a workflow for achieving 2D high-fold data by merging datasets collected in different time periods along the same profile.
(2) Designing a sparse 3D reflection seismic survey to illuminate the iron-oxide mineralization and other steeply-dipping structures.
(3) Recognition of diffraction patterns with supervised deep-learning algorithms, even when the diffraction signal is incomplete.
(4) A 3D traveltime modelling of tip diffraction response for verification and estimation of their origin.
(5) Using unsupervised deep-learning algorithm coupled with Hough transform for improved delineation of diffraction.

In terms of novelty and originality, the studies build on each other and have a continuity. They have all been attempted for the first time either at the sites for improved geological understanding and exploration or for new solutions adapted for hardrock settings and datasets. Some of the algorithms can be applied to other datasets or implemented in routine processing, modeling and interpretation workflows.

1.2 Outline of the thesis

This thesis consists of eight chapters, summarizing theoretical background of the methodologies used for the research in the thesis and their practical applications in a form of case studies. *Chapter 1* introduces the topic and describes the motivation and objectives of the thesis. In *Chapter 2*, geology of the mineral deposits studied in the thesis is provided. *Chapter 3* describes the refection seismic methods and their applications for mineral exploration, including advanced methodologies for pre-stack data processing. In *Chapter 4*, a theoretical background on diffraction response and deep-learning algorithms applied to recognize and denoise diffraction as response of some mineral deposits is presented. Four papers presented in this thesis are summarized in *Chapter 5*. Conclusions of the thesis are given in *Chapter 6*. In *Chapter 7*, future research possibilities and works based on the used methodologies and findings are described. Thesis summary in Swedish is provided in *Chapter 8*.

Attached to a hardcopy of the thesis are the four papers, of which three are published and one is in revision. Only a short summary of the papers is provided in the online and public thesis (*Chapter 5)*. In **Paper I**, two datasets from two different campaigns of 2D reflection seismic surveys, collected at Blötberget mine-Sweden, were merged to achieve a high-fold dataset for imaging iron-oxide mineralization at depth. Dominant surface-waves were attenuated using the fast discrete curvelet transforms, allowing an improved reflec-

tion image of the mineralization. The obtained results showed possible mineralization extension with depth beyond the known dimension from existing and historical boreholes and helped justifying planning the sparse 3D survey presented in **Paper II**. The results of the sparse 3D survey showed that it was possible to image the iron-oxide mineralization and its extensions laterally and with depth, despite the narrow azimuth-offset coverage and possibly some acquisition footprints. The sparse 3D survey also provided interpretation of additional potential resources and possible fracture/folding systems that control the 3D geometry of the deposits. **Papers III** and **IV** illustrate the possibility of using supervised and unsupervised deep-learning algorithms for recognizing diffraction patterns, primarily in hardrock seismic data.

This thesis contributes to the development and application of seismic methods in hardrock settings by making a step towards improved imaging and delineation of mineral deposits and providing targets for future exploration programs. The learning lessons and the experiments presented in the thesis are useful for both the academic world but also industry; an essential element of the Smart Exploration™ project but also a contribution to raw materials security and sustainability.

2 Targeted deposits

The case studies presented in this thesis are from three sites, Blötberget (in the Ludvika Mine) in central Sweden, and Halfmile Lake (deep zone) and Matagami (Bell Allard) in eastern Canada. The targeted deposits are iron-oxide and VMS and all occur within a crystalline or hardrock (high > 5500 m/s background velocity) geological setting (Figure 2.1).

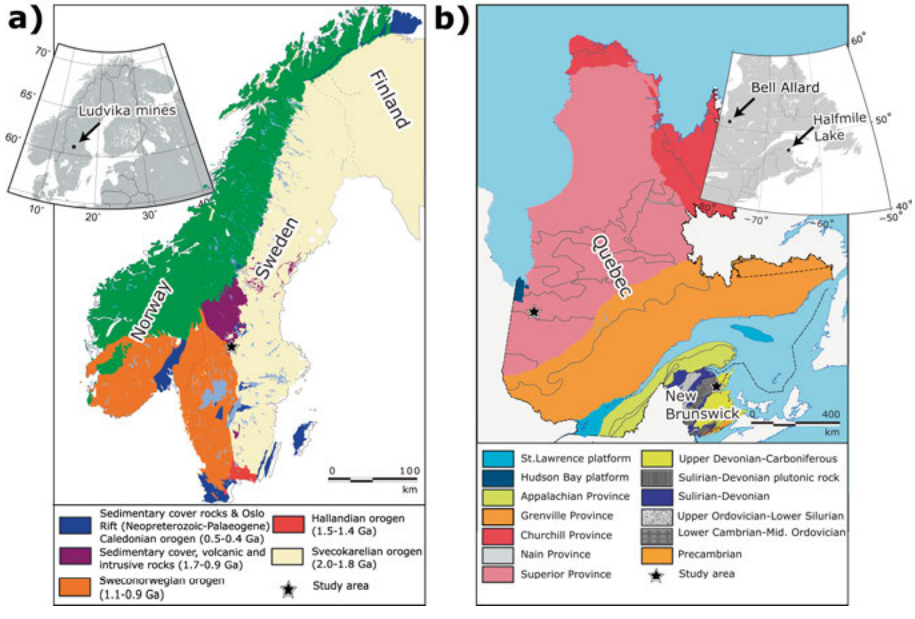

Figure 2.1. Simplified geological maps of (a) Sweden (Ludvika Mines) and (b) eastern part of Canada (Quebec, Matagami deposits, and New Brunswick, Halfmile Lake deposits) with the black stars showing the study sites. Geological maps are obtained from the Geological Survey of Sweden and Geological Survey of Canada.

Papers I and **II** focus on the iron-oxide mineralization in the Bergslagen mineral endowed district in south central Sweden within the so-called Ludvika Mines where numerous other types of deposits also are present. Bergslagen belongs to the Svecokarelian orogen with metamorphosed volcano-sedimentary host rocks of Paleoproterozoic (1.8-1.95 Ma) age (Allen et al., 1996; Jansson and Allen, 2011; Magnusson, 1970; Ripa, 2001; Stephens et al., 2009).

Rocks in Bergslagen and in the Ludvika Mines are high deformed and have experienced several stages of folding, faulting, and reactivations (e.g., Malehmir et al., 2011).

The VMS deposits in Halfmile Lake, **Paper III**, are in the Bathurst mining camp in New Brunswick, Canada. The site is well known for the hardrock reflection seismic community because it allowed a major seismic campaign to provide a drill target that led to the discovery of a blind deposit, deep zone, at a depth of 1200 m (Matthews, 2002). Major tectonic activities in the Bathurst mining camp are from Ordovician to Jurassic periods emplacing most of the VMS deposits (Staal et al., 2003).

The VMS deposits in the Matagami mining district, **Paper IV**, in Quebec, Canada occur within the Superior province and are part of the Archean Abitibi greenstone belt. The belt endowed not only with base-metal deposits but also host some of the richest gold deposits in the world. Bell Allard VMS deposit within the Matagami district, studied within this thesis, belongs to a complex geological setting where several dykes and sills complicate its seismic response; it occurs within one of three major felsic-dominated structural packages (Debreil et al., 2018) where faults and folds do not allow a good marker for their easy deep-targeting through structural tracking.

2.1 Blötberget iron-oxide deposits

The iron-oxide deposits at Blötberget (Ludvika Mines) mining site in the Bergslagen district are known for their high-quality and low impurities with disadvantaged, e.g., heavy metals, minerals. The largest deposits are believed to be magmatic or from high-temperature fluids and have some apatite. The iron-oxide mineralization comprises magnetite and hematite with over 50% of iron content. The measured and indicated mineral resources are estimated to be 45.4 Mt with 41.7% iron and 9.6 Mt with 36.2% iron, respectively. Inferred mineral resources are estimated to be 11.8 Mt grading 36.1% iron (Lowicki, 2017). Additional potential mineral resources in the downdip extension of the known mineralization are inferred from the sparse 3D reflection seismic survey (**Paper II**) and estimated to be on the order of 10 Mt, yet to be confirmed with drilling programs (Malehmir et al., 2021). The iron-oxide mineralization is composed of two main sheet-like horizons, whose thicknesses vary approximately from 10 to 35 m. Figure 2.2 shows an example downhole log of magnetic susceptibility, density, and sonic velocity of one of the boreholes intersecting the mineralization. Synthetic seismograms generated from these logs suggest strong seismic response from the deposits and why seismic methods can be useful for their deep targeting (Maries et al., 2017).

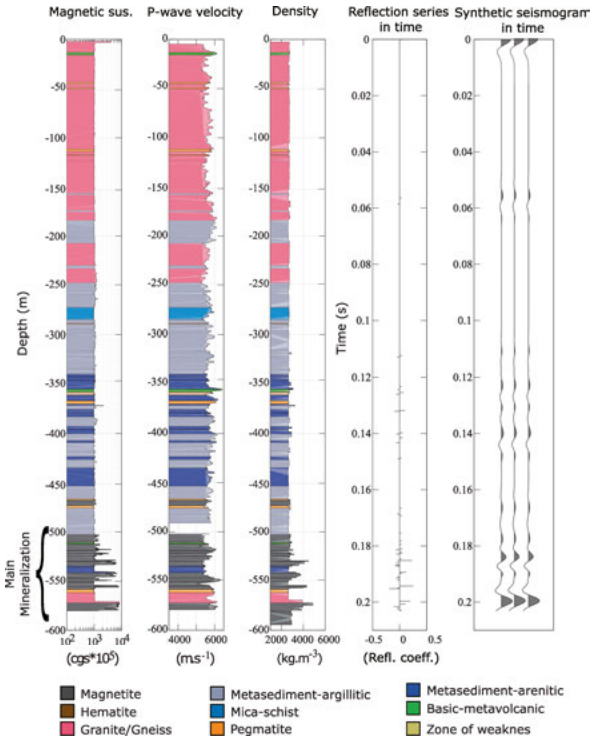

Figure 2.2. Physical properties logs from one of the boreholes intersecting the Blötberget deposits at approximately 500-550 m depth. Based on Maries et al. (2017).

2.2 Halfmile Lake and Bell Allard VMS deposits

Most VMS deposits occur in submarine volcanic or volcano-sedimentary settings, and they are major sources of copper, zinc and lead worldwide and in some places, they also host significant amount of silver and gold (e.g., Galley et al., 2007). They usually appear in the form of sulphide mounds or lenses, but they can also be stinger or stockwork depending on their distant from the volcanic/hydrothermal vents. The present analogue to land VMS deposits is found near the mid ocean ridge forming the so-called seafloor massive sulphide (SMS) deposits from the black smokers (e.g., Boschen et al., 2013).

Halfmile Lake deposits in the Bathurst mining camp were formed within a volcano-sedimentary setting, and due to the overturn of the lower to middle Ordovician Tetagouche Group, three different sulphide lenses can be distinguished: upper, lower and deep zones. Historically, these deposits were found using various exploration methods. The Upper zone was nearly exposed and discovered using grassroot exploration techniques (e.g., soil sampling and drilling), while the lower zone was discovered at 600-800 m depth using deep-

probing electromagnetic methods. The deep zone was discovered in 2002 using 3D seismic methods (Matthews, 2002). For the case study within this thesis the deep zone deposit was considered as it shows a pronounced diffraction response in the 3D seismic data (Malehmir and Bellefleur, 2009) It consists of pyrrhotite breccia and stockwork led-zinc-copper sulphide minerals. The measured and indicated mineral resource estimates of the deep zone is 7.8 Mt, grading 6.94% zinc, 2.35% lead, 0.18% copper, 36 g/t silver and 0.30 g/t gold (Budulan et al., 2015). The deep zone is still intact and economically still unviable. Sonic velocity, density, and impedance logs from one of the boreholes that intersects the deep zone lens is shown in Figure 2.3a. Synthetic seismograms generated from these logs suggest strong seismic response from the deep zone and why the 3D seismic survey was successful for its targeting.

The Bell Allard VMS deposit in the Matagami mining district is formed at the interface of the Watson Lake Group, comprising of dacites and rhyolites, and Wabassee Group, characterized by basaltic volcanism with subordinate felsic activity, accompanied with mafic-dominated intrusions (Debreil et al., 2018). The deposit consists of two lenses of which the north lens is composed of high-quality Zn-rich massive sulphides. The reserves based on a drilling campaign in 1994 and while the mine was still active were estimated to be 3.2 Mt grading 13.77% zinc, 1.50% copper, 43.45% g/t silver and 0.76 g/t gold (Adam et al., 2003) Sonic velocity, density, and impedance logs from one of the boreholes near the Bell Allard deposit are shown in Figure 2.3b. They show that major changes in P-wave velocity and density come from lithological variations hence the host rock can be strongly reflective. This is correct as the diffraction response of the Bell Allard deposit is strongly overprinted by numerous reflections making its delineation and separation difficult.

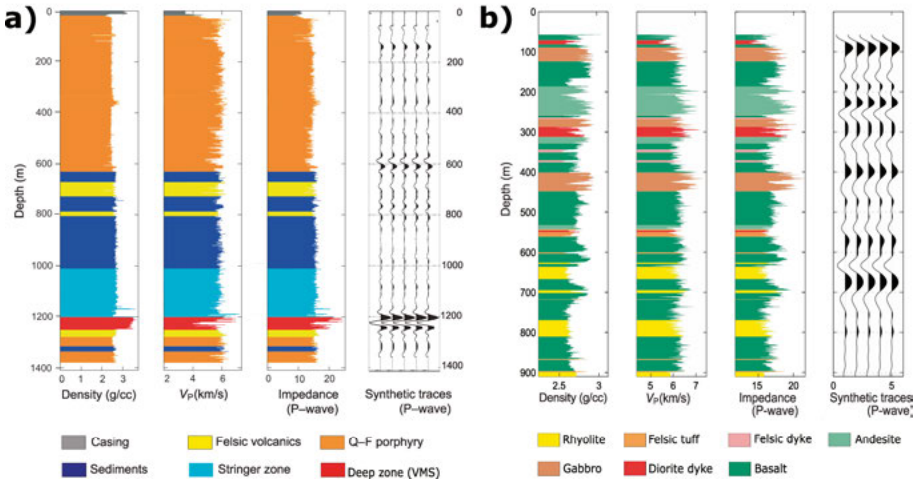

Figure 2.3. Sonic velocity, density, and impedance logs from (a) Halfmile Lake deposit from a borehole intersecting the deep zone sulphide lens and (b) a borehole near the Bell Allard deposit showing that the VMS deposits and lithological changes can generate a strong seismic response. Based on Malehmir and Bellefleur (2009) and Calvert et al. (2003), respectively.

3 Reflection response of mineral deposits

Reflection seismic method for mineral exploration and in hardrock settings has increasingly been used because of its ability to provide high-resolution subsurface images (Bellefleur et al., 2004; Cheraghi et al., 2012; Koivisto et al., 2012; Malehmir et al., 2017). Pioneered mainly by South African and Canadians (Adam, 1997; Adam et al., 2003a; Adam et al., 2003b; Manzi et al., 2020; Milkereit et al., 1996; Milkereit et al., 2012; Roberts et al., 2003), the methodology quickly expanded to Europe, Australia, and other places in the world (Heinonen et al., 2012; Kukkonen et al., 2012; Malehmir et al., 2006; Malehmir et al., 2012; Markovic et al., 2020; Urosevic et al., 2007). The breakthrough was the successful and systematic experiments in the Halfmile Lake for VMS targeting and improved structural understandings in the world-class gold deposits in the Witwatersrand basin (e.g., Campbell and Crotty, 1990). When the deposits have a high seismic impedance contrast (product of velocity and density), reflection response can straightforwardly be distinguished from the host rocks. While appearing simple, the complexity of hardrock environments can challenge this delineation due to various reasons such as heterogeneity, lack of marker reflections and the most problematic one, out-of-the-plane structures that are often short in length. It is therefore obvious why many algorithms and workflows have been developed to tackle these issues (e.g., Balestrini et al., 2020; Brodic et al., 2021; da Col et al., 2020; Donoso et al., 2021).

The first part of this thesis (**Papers I** and **II**) illustrates the potential of employing 2D and sparse 3D reflection surveys for imaging iron-oxide deposits beyond their known, from boreholes, dimensions. The first 2D survey was justified since the results of two other experiments in Sweden showed targeting iron-oxide deposits are possible (Malehmir et al., 2011; Place et al., 2015). The new survey was placed and conducted along the dip direction of the mineralization, and although having a low-fold coverage, the deposits showed strong reflection response encouraging further field campaigns. To improve the fold coverage, along the same profile another dataset was acquired and by combining the two datasets, reflection response of the deposits showed continuous response with depth. Lateral dimensions and additional potential resources were estimated from the follow-up sparse 3D survey, which was planned based on the 2D studies. Worthwhile mentioning that the experiments at the site were conducted in a systematic manner including downhole surveys,

among other geophysical methods, allowing improved interpretations and planning works. Given the success of the surveys, a brief description of methodologies and challenged encountered with 2D and 3D surveys are covered in this chapter for completeness purpose.

3.1 High-fold 2D data concept

The workflow developed within this thesis (**Paper I**) for increasing the resolution and signal-to-noise ratio (trace density) is showcased through merging of the data acquired along the same profile but in different times and using different types of recorders (the seismic source was identical). The goal of developing such a workflow was to test if the reflection response of the iron-oxide mineralization can be imaged better with depth compared to the results obtained from only one of the datasets e.g., the one of the landstreamer along by (Malehmir et al., 2017b) or separate data of the 2016 survey. Prior to merging of the datasets, each dataset was pre-stack preprocessed separately, including refraction static corrections given that the position of the receivers and shot points differ in the field campaigns (e.g., landstreamer on the road and wireless recorders on the ditch). After merging of the data, only on a portion of the data, where the mineralization response was visible in the shot gathers, curvelet transform was applied to suppress surface-waves and enhance the reflections.

Comparison of the results from unmigrated sections, before and after merging the datasets, are shown in Figure 3.1. Merged data (Figure 3.1c) show continuous reflections from the mineralization with depth; it is also possible to note a possible underlying, a couple of hundred meters, reflection. To verify that the high fold helped by merging of the two datasets, RMS amplitudes were calculated in windows above and within the mineralization reflective zone at a given CDP range.

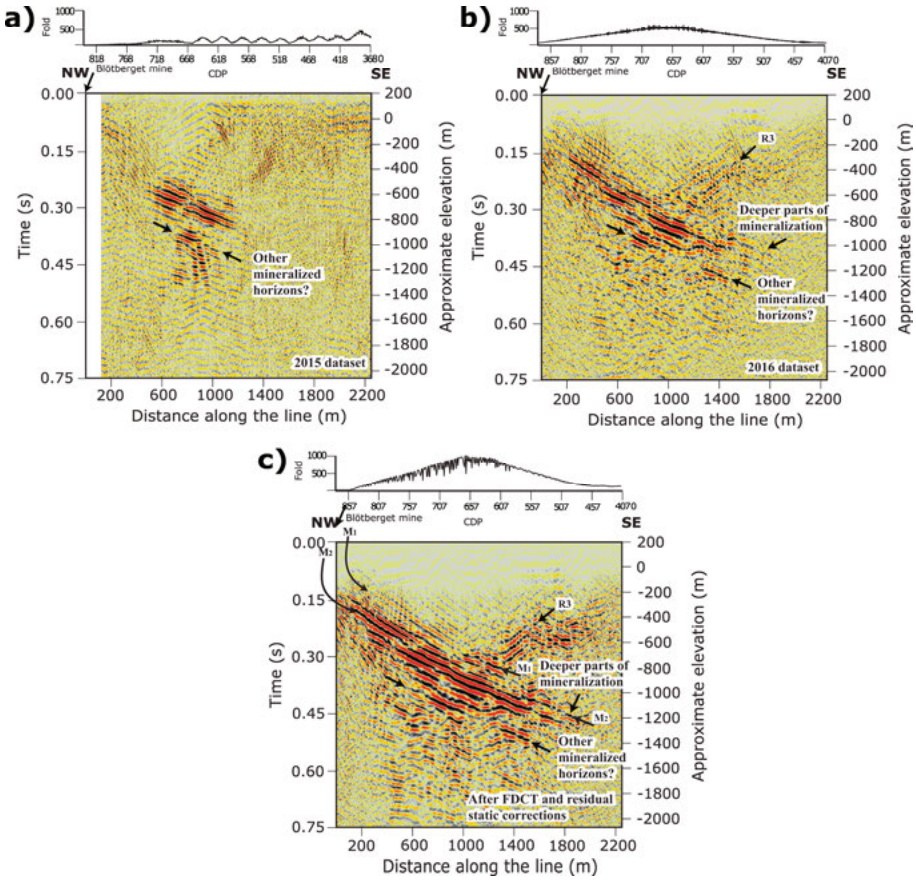

Figure 3.1. Unmigrated stacked sections of (a) a portion of the 2015 dataset, (b) the whole 2016 dataset, and (c) portion of the merged datasets after curvelet transforms and residual static corrections. The CMP fold plots are shown for each section. Black arrows mark mineralization horizons M1 and M2, their extension with depth and possible underlying resources. Reflection R3 is interpreted as a possible fault structure.

3.1.1 Fast Discrete Curvelet Transform for surface wave attenuation

The curvelet transform is a multi-scale and multi-directional transform to sparsely represent two or more-dimensional data and originates from the image denoising domain (Candès and Donoho, 2004; Candès and Guo, 2002; Starck et al., 2002). The construction of curvelets occurs in the frequency domain, with radially and angularly constrained windows (Candès et al., (2005) for the mathematical derivations). The inverse Fourier Transform of such a wedge in the frequency domain then yields a so-called "mother" curvelet (φ_j) of scale 2^{-j}, which is oscillatory in one direction and smooth in another. In

the oscillatory direction, a curvelet resembles a wavelet (usually the Meyer wavelet), and in the smooth direction, the curvelet is spatially defined by a Gaussian function. This spatial Gaussian constraint ensures a good localisation, in terms of the uncertainty theorem, in both spatial- and frequency-space, i.e. the phase-space (Donoho and Stark, 1989). This "mother" curvelet (φ_j) is then subsequently translated and rotated to represent a function as a linearly weighted combination of curvelets. These weights are termed the curvelet coefficients (c) and defined as the inner product of a function $f \in \mathrm{L}^2(\mathbb{R}^2)$ with a curvelet (φ):

$$c(j,l,k) \equiv \langle f, \varphi_{j,l,k} \rangle = \int_{\mathbb{R}^2} f(x)\overline{\varphi_{j,l,k}(x)}dx \quad , \tag{1}$$

with translations (k) and rotations (l) of the "mother" curvelet (φ_j) of scale 2^{-j}. The curvelet transform is a tight frame, in that any function $f \in \mathrm{L}^2(\mathbb{R}^2)$, can be represented as a combination of curvelets. An example of a 2D curvelet in the spatial and frequency domain is shown in Figure 3.2. In the frequency domain (Figure 3.2c), the curvelet comes in the form of two angular wedges around the origin. Curvelets can be of different scales and angular directions, stemming from their construction in the frequency space (Figure 3.2c). In this example, the curvelet is of scale 3, represented by the third square frame in the frequency domain, and has an angular direction of approximately -45° (controlled by the angular wedges).

Curvelet denoising procedure is usually applied in the following steps: (1) the forward curvelet transform is applied, which decomposes the seismic image into different scale and angular curvelet coefficients in the curvelet domain, (2) subsequently, threshold, or modify, the curvelet coefficients, and (3) finally the inverse curvelet is performed to obtain a noise attenuated seismic image.

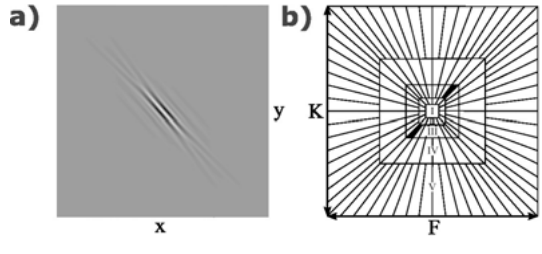

Figure 3.2. A curvelet is shown both in (a) spatial domain and in (c) frequency domain, where the curvelet comes in the form of two wedges around the origin. This curvelet is of scale 3, with the other scales indicated by roman numerals, in this example from scale I to scale V. For every other scale, the number of angular wedges doubles, which is due to the second dyadic coronae structure (based on von Ketelhodt et al., 2019).

In practice, curvelet transforms are widely applied for attenuation of coherent and incoherent events, both in shot gathers and stack sections (Buntin et al., 2019; Górszczyk et al., 2014; Naghizadeh and Sacchi, 2018; Neelamani et al., 2008). In **Paper I,** curvelet transform was applied to attenuate strong surface-waves in combination with a bandpass filter. Before applying the curvelet transforms, data were LMO corrected to minimize the artefact effects due to irregular receiver spacing. Denoising was applied on each shot gather separately where in general for the thresholds, 6 scales were chosen with angular range 65º to -75 º on the right-hand side and 107 º to -117 º on the left-hand side of the shot gathers. After denoising, the inverse LMO was applied. An example of the curvelet denoising and difference when applying only bandpass filter is shown in Figure 3.3.

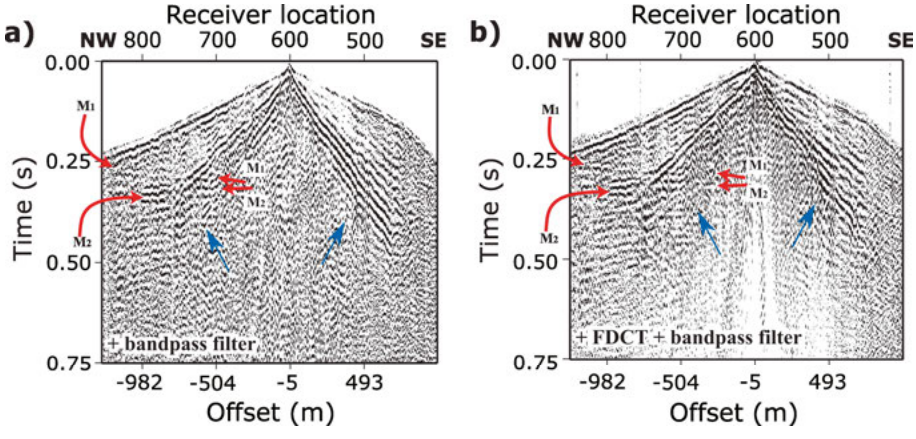

Figure 3.3. An example shot gather from the 2016 survey, and comparison of the surface-wave attenuation when (a) only bandpass is applied and (b) when FDCT is applied in combination with the bandpass filter. In (b), the mineralization horizons M1 and M2 can be better distinguished with slightly different dip directions. This shear-wave arrival appears more linear and easier to remove using for example median filters.

3.2 Sparse 3D reflection seismic survey

A sparse 3D reflection survey is not a usual, nor should ever replace, when possible, choice in 3D survey design. However, in certain scenarios can provide suitable information on subsurface structures especially if it is designed based on the previous knowledge and target geometry. This can save the budget and limit environmental impacts. Within the scope of this thesis (**Paper II**), a sparse 3D survey was conducted with the primary goal of imaging the iron-oxide mineralization at depth and its lateral extensions. The study site

is located within extensive forests; hence all forest and major roads were utilized for deployment of sensors and source operation. In particular roads with an orthogonal angle to the strike of mineralization were given a priority.

The planned survey, based on the several scouting campaigns is shown in Figure 3.4a. It displays the fold coverage for a bin size of 10 m and positions of receivers and shot profiles. The planned survey had a uniform offset-azimuth coverage as well as fold (Figure 3.4b). As the seismic source was a 32t vibro-truck, that influenced on survey layout modifications because some roads did not have enough stability, or they were not permitted for vehicles over 11t. The executed survey and fold coverage are shown in Figure 3.4c. Although a narrow offset-azimuth was achieved, the direction was favoring the dip direction of the mineralization. This implies some acquisition footprint and must be carefully noted when interpreting such a dataset. Imaging complications are another item to note as the dataset would have irregular offset several processing steps such as DMO corrections and stacking.

In any 3D survey, the size of the target to be resolved and the signal quality need to be carefully designed. Smaller shot and receiver spacing and higher folds, the improved resolution and signal quality (to a certain point). Bins are designed on this basis and can be regular or irregular for sparse 3D data. Irregular bins have a disadvantage of introducing smoothing effects hence resolution (e.g., Vermeer, 2010). The chosen bin size in the case of 3D sparse dataset is 10 m. Considering sweep parameters (10-160 Hz), dip of the reflector (e.g., mineralization) and a mean velocity of a hardrock medium, the maximum non-aliased bin size was calculated using the equation (Yilmaz, 2001):

$$\Delta x \leq \frac{v_{rms}}{4 f_{max} sin\alpha} \quad , \tag{2}$$

where Δx represents the 3D bin size (regular). It is important to point out that hardrock settings imply high frequency contents, compared to sedimentary settings, therefore if larger bin sizes are used, a maximum non-aliased frequency would be too low. This implies lowering resolution.

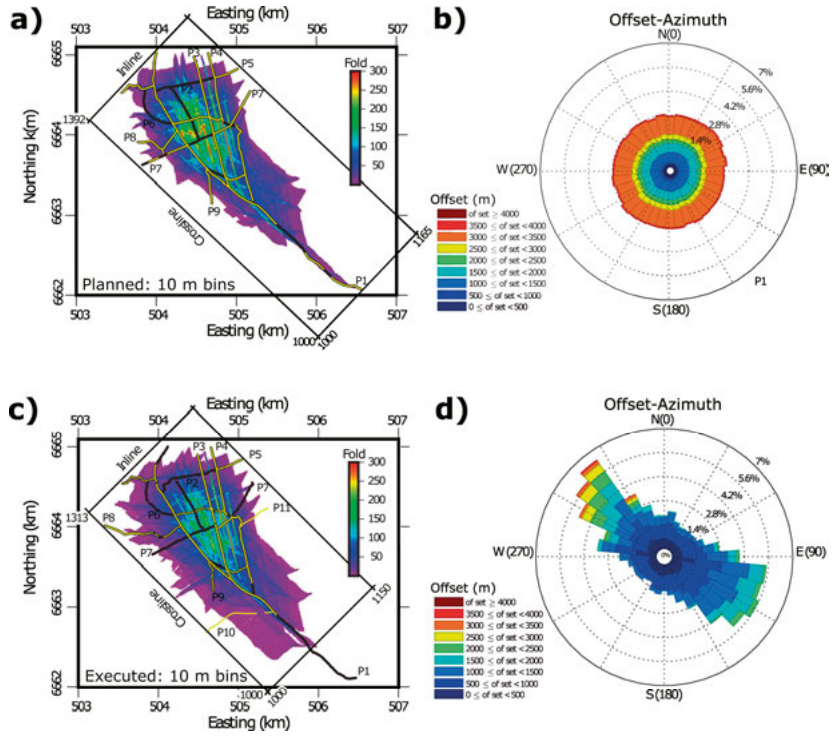

Figure 3.4. The overall fold coverage of (a) planned and (c) executed 3D seismic surveys at Blötberget. Chosen bin size is 10 m given the thickness of the mineralized horizons. Offset-azimuth plot in (b) shows a uniform coverage for the planned, while (d) a narrow offset-azimuth distribution for the executed survey. The survey, however, covers the NW-SE area, overlapping the dip direction of the mineralization.

An inline, crossline and timeslice example from the unmigrated volume of the 3D sparse dataset is shown in Figure 3.5. The results show strong reflection response of the mineralization and possible folding and faulting structures. While one anticipates some acquisition footprint in the data, it is not as obvious probably because of the strong reflection response of the mineralization making this recognition difficult. Despite sparsity, the obtained results provide extended knowledge on the mineralization extensions laterally and with depts. Further research should be possible for regularizing (e.g., Cheraghi et al., 2012) the dataset in terms of offset and azimuth and if for example a random 3D survey would have been more ideal.

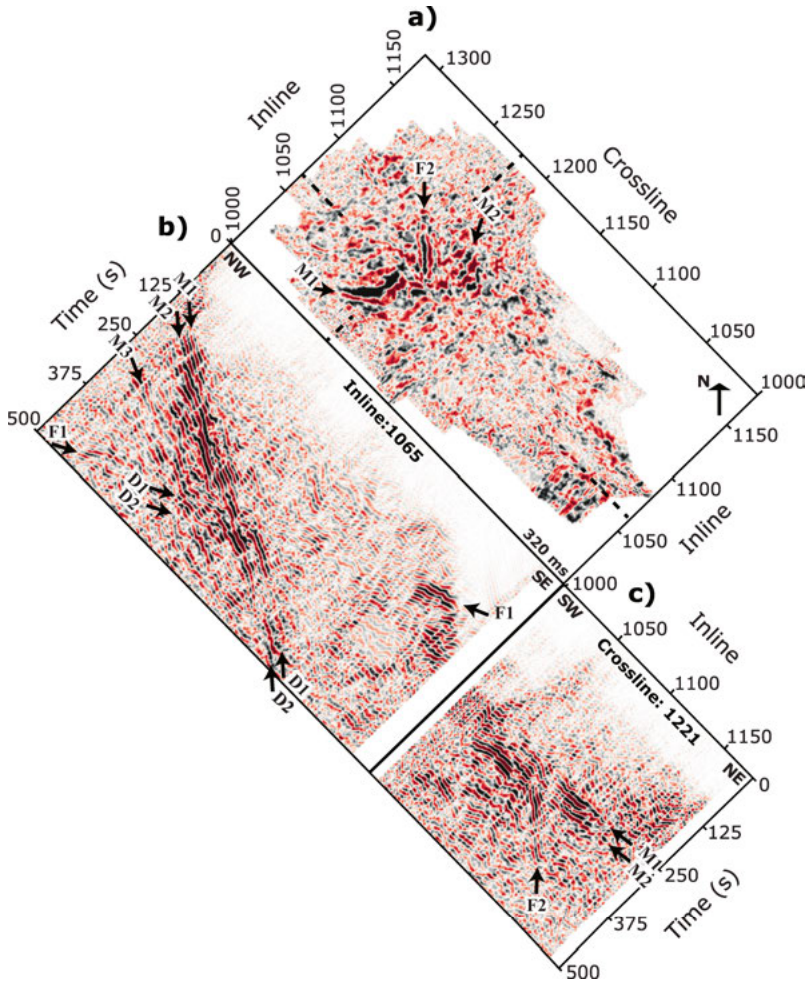

Figure 3.5. The unmigrated stacked volume of the sparse 3D dataset showing the iron-oxide mineralization signature and interpreted fault/fold systems (F1 and F2 and diffraction responses D1 and D2) at different (a) timeslice, (b) inline and (c) crossline. In correlation with the 2D sections (Figure 3.1), one can track the mineralized horizons M1 and M2 and distinguish them clearly in the crossline view. It was possible to image the mineralization in 3D even with a sparse, narrow offset-azimuth, seismic data implying major budget saving and reduced environmental impact.

4 Diffraction response of deposits

Diffraction wavefield studies became of interest because diffraction signal provides information about not only small and medium-scale objects but also a possibility to study lithological and structural composition of the subsurface including the degree of anisotropy and heterogeneity (e.g., Landa and Keydar, 2012; Lin et al., 2018; Malehmir and Bellefleur, 2009; Schwarz and Krawczyk, 2020). For this thesis, diffraction is defined as a signal that is observable by a human eye while scattering is not. Diffraction signal can be generated from a point or tip of an object like intrusions or isolated bodies, or from an edge like faults. When a seismic wavefront hits the tip of a point-like object, diffraction propagates radially in all directions (Figure 4.1a). When it hits the edge of an object, for example if it propagates obliquely to a linear-shaped object, a conical diffraction forms, where the edge is their common axis (Figure 4.1b).

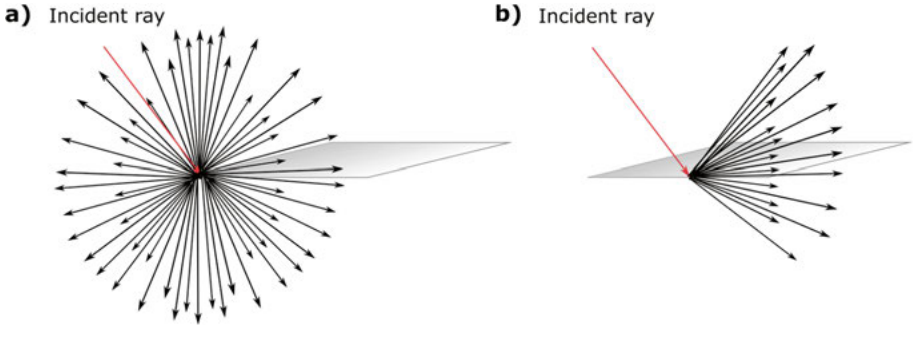

Figure 4.1. A sketch of the incident ray (red arrow) generating diffraction from (a) a tip and (b) an edge structure (modified from Rochlin et al., 2021). The tip diffraction is spherical while the edge diffraction would be conical.

The formula for diffraction traveltime calculation used for the studies covered in **Papers III** and **IV**, is the simplified approximation of a point-type diffractor at zero-offsets:

$$t_d = \sqrt{{t_0}^2 + \frac{4x^2}{{v_{rms}}^2}} \quad , \tag{3}$$

where t_0 represents time at the diffraction apex, x its CDP position or horizontal distance away from the diffractor, and v_{rms} is the root-mean square velocity of the medium.

For a set of source and receiver, the tip diffraction traveltime would follow different formulation:

$$t_d = \sqrt{\frac{{t_0}^2}{2} + \frac{x^2}{{v_{rms}}^2}} \quad , \tag{4}$$

An edge diffraction at zero offset follows the same formula as equation (1), however it requires one of the tails to have an opposite polarity. The edge diffraction at any offset and in a general term is more complex as has been researched by a few authors (Keller, 1962; Klem-Musatov, 1994; Klem□Musatov and Aizenberg, 1984). Diffracted waves from an edge can be focused at its origin (image point) where the incident ray hits the edge. To do so, the location of the cone must be defined with respect to the locations of the sources, image point and azimuth of the linear diffractor (Keydar and Landa, 2019). The following formula for computing edge diffraction response is used:

$$t_d = \frac{1}{v_1}\sqrt{D_S^2 + x^2} + \frac{1}{v_2}\sqrt{D_R^2 + (D - x^2)^2} \quad , \tag{5}$$

where D_s and D_R are distances from the source and receiver normal to linear diffractor, x and D are distances from the image point and points where source and receiver are normal to the line diffractor, respectively.

Because diffraction wavefield imaging and separation is more common in sedimentary basins (Berkovitch et al., 2009; Dell and Gajewski, 2011; Fomel, 2002; Fomel et al., 2007; Klokov and Fomel, 2012; Schwarz, 2019), in **Papers III** and **IV**, the focus was to apply deep-learning algorithms for diffraction pattern recognition and denoising on the diffraction response in hardrock geological settings. The two 3D seismic datasets available to the research and used for imaging VMS deposits were used to showcase the methodology. The two deposits, because of primarily their high density, small sizes and strong contrast with their lithological contacts generate a notable, although complex, diffraction signal (Adam, 1997; Malehmir and Bellefleur, 2009). Some diffraction responses have asymmetric shape as the object size and shape reach the so-called Mie-scattering regime; the amplitude of diffraction tail is stronger in the downdip direction of the deposit (Malehmir and Bellefleur, 2009), hence a point diffraction assumption would violate an accurate traveltime hyperbola/hyperboloid. Although a point diffraction formula was used to model diffraction traveltimes in 2D and 3D, the model represents only an approximate solution and some inconsistencies and mismatches are anticipated.

4.1 Diffraction traveltime modelling in 2D and 3D

As an example, diffraction traveltimes from the VMS deposits described in **Papers III** and **IV** were calculated using equation (3) in 2D and 3D, assuming a point diffractor. For the 2D modelling, the time and CDP position at the apex point (assumed diffraction origin) are manually determined on different inlines. The diffraction traveltime equation can be then embedded in commercial software as was done in my thesis work. Three diffraction responses at different times were chosen for the modelling (Figure 4.2). The traveltime computation allows to confirm the diffraction patterns and with input parameters adjusting, such as velocity, one can obtain the best-fitting diffraction hyperbolas.

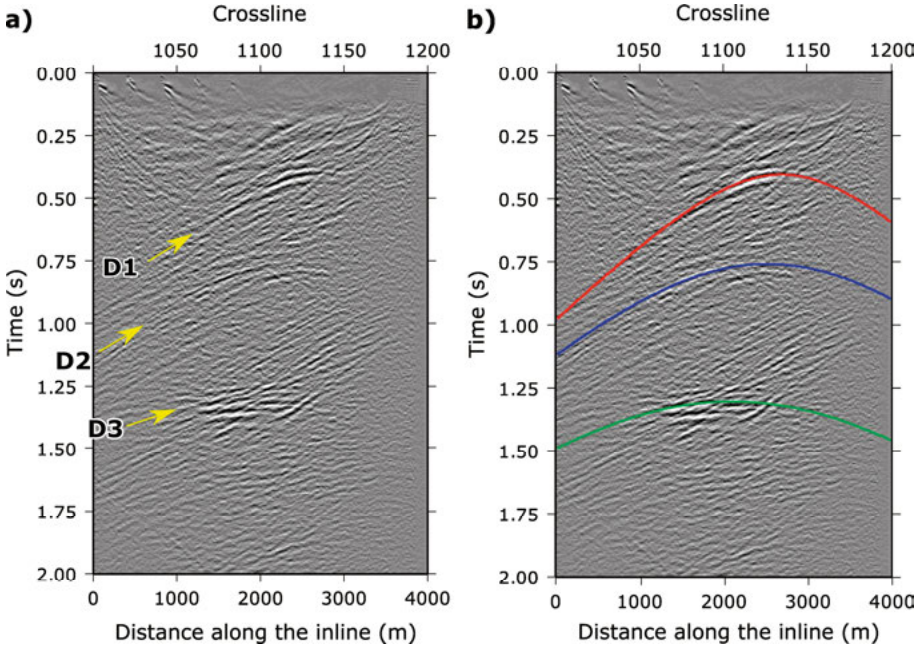

Figure 4.2. (a) An inline example from the Matagami 3D hardrock dataset and (b) diffraction traveltimes plotted over the inline at different times and from different origins.

The 3D diffraction traveltime modelling of this thesis is done in an opposite manner than the 2D diffraction traveltime modelling. In order to reconstruct a diffraction traveltime in 3D, an origin is required and sometimes this is not obvious e.g., when the diffraction is incomplete or only partly appears at the edge of the seismic volume. To be able to apply equation (3) for diffraction traveltime modelling, one has to first find the position of the apex (x,y) and subsequently calculate the time at the apex based on a pre-defined (best guess)

velocity. One way to handle this is to digitize points of the incomplete diffraction circle on timeslices and assume a response from a point diffractor. Then assuming that diffraction response on time slices should be circular, it is possible to find the origin by fitting a circle to the digitized points. Using the equation (3), it is then possible to estimate t_0 assuming a, for example, constant velocity, v_{rms} for the medium, which is not difficult in hardrock (crystalline) settings as it changes rather not anomalously (Figure 4.3).

Diffraction hyperboloid can be computed with the adaptation of the equation (3) in 3D (Figure 4.4a), as it is done in my thesis, for example, using a matrix size of 200 x 200 cells with numbers increasing from center outwards (Figure 4.4b). The obtained diffraction traveltime hyperboloid can be visualized within the seismic volume and match with the diffraction in the data even if incomplete be judged along various crosslines and inlines as well timeslices (Figure 4.4c). The 3D modelling enables reconstructing possible origin of diffraction and if they are off-plane or outside the seismic volume. In the Halfmile Lake case it was estimated to be approximately 500 m south-east from the volume, suggesting that 3D modelling, given the character of diffraction, may aid exploration of another potential VMS deposit or rather an extend 3D survey beyond the current 3D seismic volume.

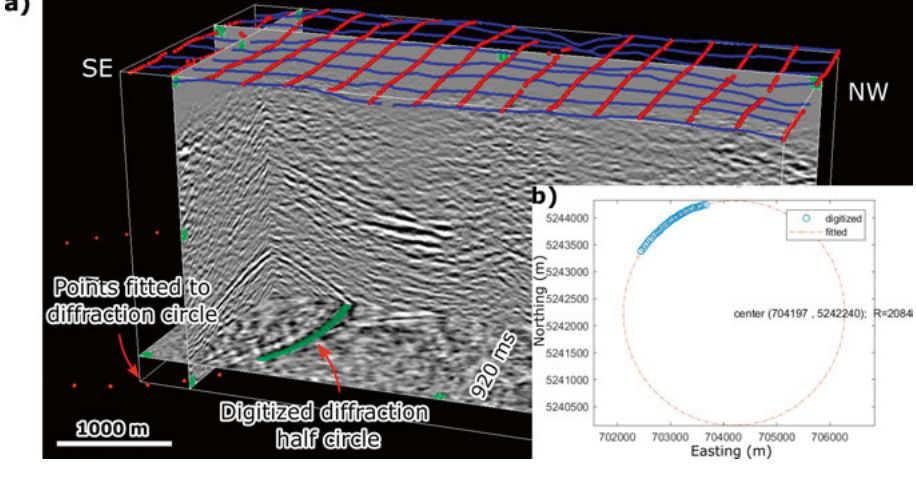

Figure 4.3. (a) 3D visualisation of the Halfmile Lake seismic volume showing the digitized points along an incomplete diffraction circle (green points). (b) The plot of the fit-to-circle calculation and obtained center (CDP position) of the diffraction. The time of the timeslice where points were digitized was used to find the apex.

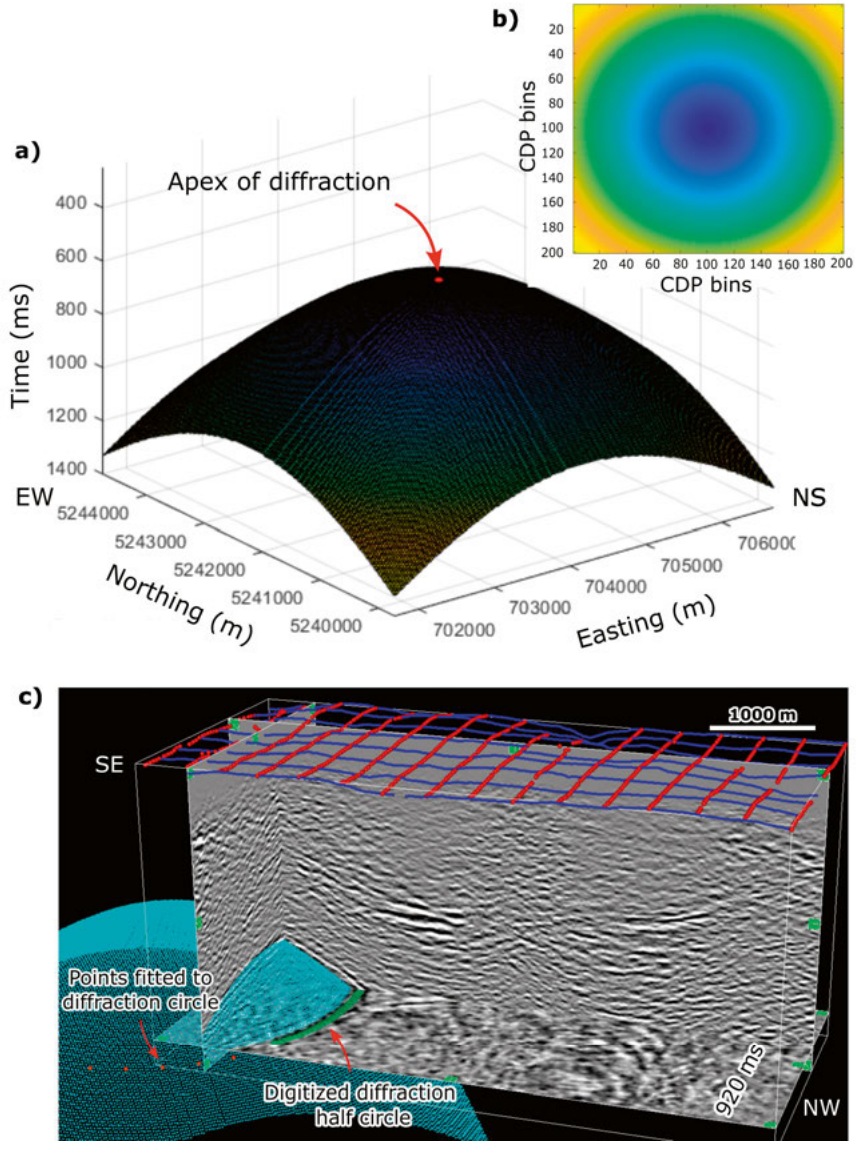

Figure 4.4. (a) Diffraction hyperboloid calculated using (b) 200 x 200 matrix (CDP bins) model. (c) Visualisation of the seismic volume where obtained hyperboloid matches the traveltime diffraction response in the timeslice, crossline and inline.

4.2 Supervised and unsupervised deep learning for diffraction recognition

Deep-learning algorithms are nowadays widely used in seismic data processing and interpretation, especially for noise attenuation, wavefield decomposition or specific geological/geophysical pattern recognitions (e.g., Birnie et al., 2021; Dell et al., 2020; Geng and Wang, 2020; Glaeser et al., 2021; Liu et al., 2022; Saad and Chen, 2020; Tschannen et al., 2020). While there are a growing number of deep-learning algorithms, they can be divided into two groups: supervised and unsupervised. Supervised learning requires, besides the original input data, a labelled representation of the data or target to be identified. This implies manual labelling of the features of the interest is required. The unsupervised learning avoids human involvement and is based on the input data figuring out its own structures; the algorithm itself correlates useful from unwanted information or signal. In **Paper III**, the supervised learning through the U-net algorithm for diffraction pattern recognition is used, while in **Paper IV**, the unsupervised learning using the autoencoder algorithm is used for similar purposes. The sketches of the U-net and autoencoder architectures are shown in Figure 4.5.

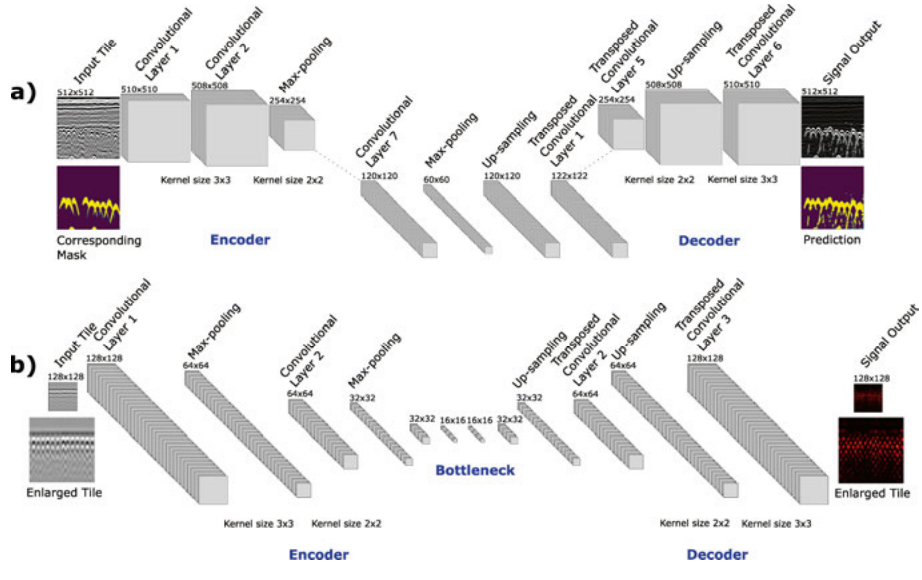

Figure 4.5. Sketch of (a) the U-net architecture, and (b) autoencoder architectures exemplified for GPR data. The sections are broken into tiles in order to increase the training data. The U-net here consists of seven convolutional layers, while the autoencoder comprises three convolutional layers. Note that the autoencoder is built on top of the U-net convolutional neural network.

For the U-net algorithm, diffraction signals are classified only. When the signal is labelled, it does not only capture the shape of the diffraction, it does as well the pixel intensity (amplitude) within the labelled diffraction. The U-net is divided in two paths: (1) encoder, where the algorithm captures the context of the object (diffraction) through several convolutional and max-pooling layers, and (2) decoder, which provides the actual position of the signal using transposed convolutional and up-sampling layers. The autoencoder architecture is built on top of the U-net where the encoder learns the best representation of the signal (e.g., as much as possible clean sections with diffraction signals) and bottleneck forces compressed knowledge representation of an input signal (latent space). The decoding part then maps back the latent space representation into reconstructed signal, which contains most useful information of the signal (Bank et al., 2020) The application of both algorithms on seismic synthetic and real GPR data where diffractions are notable and have correlated structures is straightforward, however, this is not so simple for 3D hardrock seismic datasets, where diffraction response of VMS bodies are complex and falls within coherent and consistent reflectivity that cannot be simplified by the autoencoder algorithm. Therefore, both solutions need to be developed in a tailored workflow for mineral exploration purposes.

When applying the U-net algorithm on inlines of a 3D dataset, the algorithm should be able to recognize other diffraction patterns, even incomplete ones, which are not labelled and never shown in the training data. As shown in Figure 4.6, the incomplete diffraction signal that is additionally delineated contains similar shape and pixel intensities as already labelled, known (labelled) diffraction. An added-value in this case is that given the same amplitude strength as the known diffraction, the newly-found one can be from similar geological entities (e.g., a VMS deposit) although situated deeper than the known one.

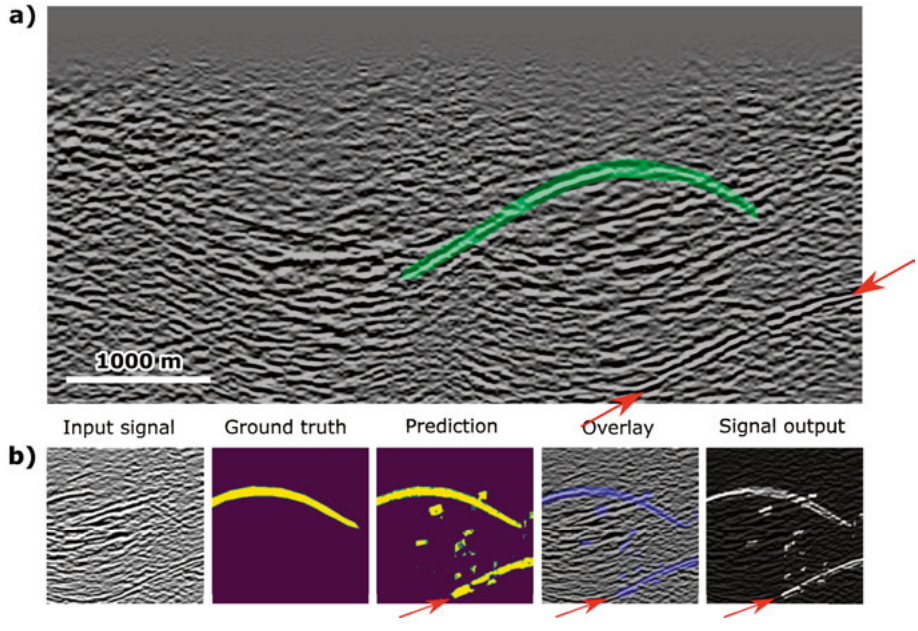

Figure 4.6. (a) An example inline used for the training of diffraction. The green-shaded area represents the labelled diffraction. (b) An example of one of the tiles, where beside the known diffraction, another, incomplete diffraction signal is predicted. Red arrows point at the never labelled, but delineated, diffraction from the supervised deep-learning workflow.

To exemplify the application of autoencoder workflows, another 3D hardrock seismic dataset is used here where again a diffraction signal is associated with a major VMS body. Due to low signal-to-noise ratio, it is not possible to obtain denoised diffractions from the inlines because the algorithm correlates together both reflection and diffraction signals as required minimally to explain the data after the encoding part. The timeslices, however, show distinctive circular-shaped diffraction compared to reflections and are better suited for the denoising workflow. Now, the autoencoder provides suppressed reflections (Figure 4.7). Nonetheless, additional edge detection tools can complement this.

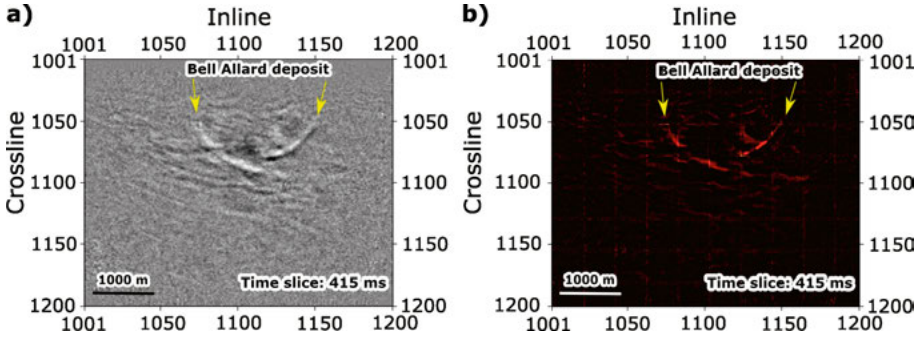

Figure 4.7. An example diffraction signature on (a) original timeslice and (b) autoencoder solution used for its denoising. An inset of the autoencoder solution with added gain is shown for visualization purposes. Yellow arrows mark the diffraction circle, a response from a major VMS deposit.

4.3 Coupling Hough transform with deep learning for diffraction delineation

Hough transform is usually applied for semi-automatic detection of linear and circular features. In a geological sense, they are mainly used for fault/fracture system detection or salt bodies (e.g., AlBinHassan and Marfurt, 2003; Chen et al., 2018; Jacquemin and Mallet, 2005; Orozco-Del-Castillo et al., 2011; Wang and AlRegib, 2014). The input parameters for the straight-line detection include the range of the dip angle of the line (angle θ between the x axis and the line r that perpendicularly connects origin O and the straight line) and the number of lines to be detected (Figure 4.8a). The line is detected based on a voting principle and the best candidates, that fits the input parameters, are chosen.

For the circle detection, the input parameter is the radius r of the circle (or range for different circle sizes) one wants to detect. To be able to perform the circle detection, an edge detection filter needs to be applied prior to the Hough transform. Once the edge of the curve is detected, the algorithm draws a circle with radius r and where most of the circles intersect will be the center of a delineated circle as is voted most (Figure 4.8b). The number of detected circles can be set to optimize solutions.

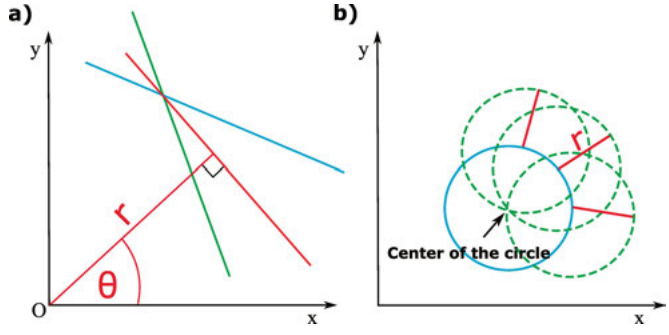

Figure 4.8. A sketch of the Hough transform principle for (a) straight-line detection and (b) circle detection. Targets are red line and blue circle. Parameters are shown in red.

These two different principles can be implemented for removing any remaining coherent noise in seismic data and direct circle detection on timeslices, as presented also in **Paper IV**. An example diffraction circle detection from the known Bell Allard VMS deposit is shown in Figure 4.9. The results show that the least solutions were obtained on the autoencoder denoised time slice, suggesting that the autoencoder solution provides a more isolated diffraction circle and is convenient for narrowing down the choices for circle delineation using the Hough transform.

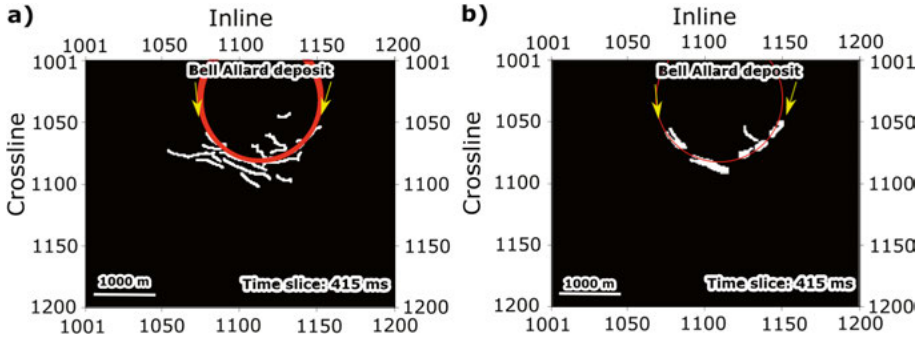

Figure 4.9. The edge detected (a) original and (b) autoencoder denoised timeslices with detected diffraction circles using Hough transform. The autoencoder denoised diffraction provides a single-circle choice.

5 Summary of papers

5.1 **Paper I:** Deep reflection seismic imaging of iron-oxide deposits in the Ludvika mining area of central Sweden

Two 2D reflection seismic datasets were acquired in two field campaigns (2015 and 2016) along the same profile at Blötberget site in south-central Sweden in the Ludvika mining area. To maximize the value of both datasets for iron-oxide mineralization imaging, they were merged to achieve a high-fold, long offset dataset. The merging of the data provided not only sharper reflections, but also helped imaging reflections at depth and speculate on crosscutting reflections to be from fault systems intersecting the mineralization.

5.1.1 Synopsis

Blötberget in south-central Sweden was historically one of the most important iron ore mines in the region. The recent trend of the iron ore needs on the market, renewed the interest to again explore for these deposits and Blötberget iron-oxide mineralization was one of the targets of investors. The 2015 campaign was designed to validate a state-of-the-art landstreamer acquisition system (Brodic et al., 2015; Malehmir et al., 2017b), whether it was possible to image mineralized horizons at all. The 2016 seismic campaign focused on employing conventional survey layout with the purpose of imaging the mineralization beyond the known depth from existing boreholes. It also aimed to provide some information about their possible lateral extensions (Maries et al., 2020); a short crossing profile was also simultaneously acquired. The layout of both surveys is shown in Figure 5.1. The workflow was developed for high-fold imaging as it was decided to merge the 2015 and 2015 datasets. To avoid the complications when calculating refraction static solutions, refraction static corrections were applied separately prior to merging the datasets. Later, part of the workflow included removal of the strong surface-wave noise using the fast discrete curvelet transforms. An example shot gather from the 2016 field campaign is shown in Figure 5.2. In the raw gather, it was already possible to observe the strong mineralization signature and with the application of the denoising algorithms, it was better possible to distinguish potentially two mineralized horizons (Figure 5.2d).

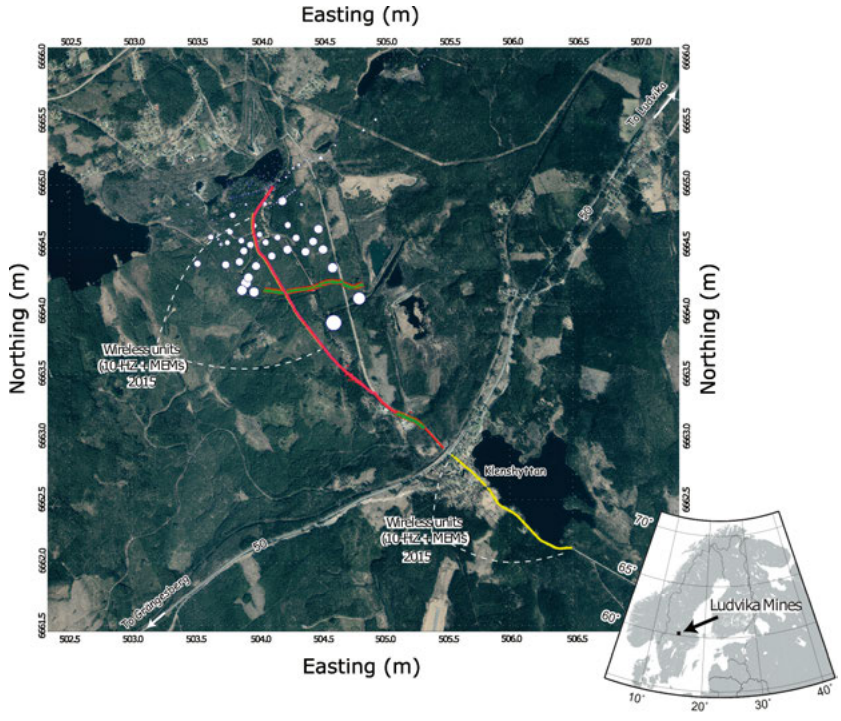

Figure 5.1. Aerial map showing the 2015 and 2016 seismic survey layouts (yellow and red dots, respectively). Both surveys were carried out along the same road, although the survey in 2015 continued over a major road and was longer. The data in 2015 were collected using a MEMS-based landstreamer array and a limited number of 10 Hz geophones connected to wireless recorders (totally 51 positions). The 2016 field campaign only employed 10 Hz geophones connected to cabled and wireless recorders (totally 451 positions).

The unmigrated stack of the merged datasets is shown in Figure 5.3. The two mineralized horizons can be observed and the extension of the reflections with depth suggests that mineralization is continuous beyond what the 2015 survey showed (Malehmir et al., 2017b). Few other reflections were observed in addition to the ones corresponding to the mineralization. The first one is an underlying to the known mineralization reflection, which possibly marks a deeper mineralized horizon. Another three cross-cutting reflections, dipping to the northwest were interpreted as faults or less likely additional resources, due to their similar amplitude character. However, they lack reflection continuity due to low-fold coverage in the part where the profile crosses the major road and it is difficult to provide any reliable interpretation.

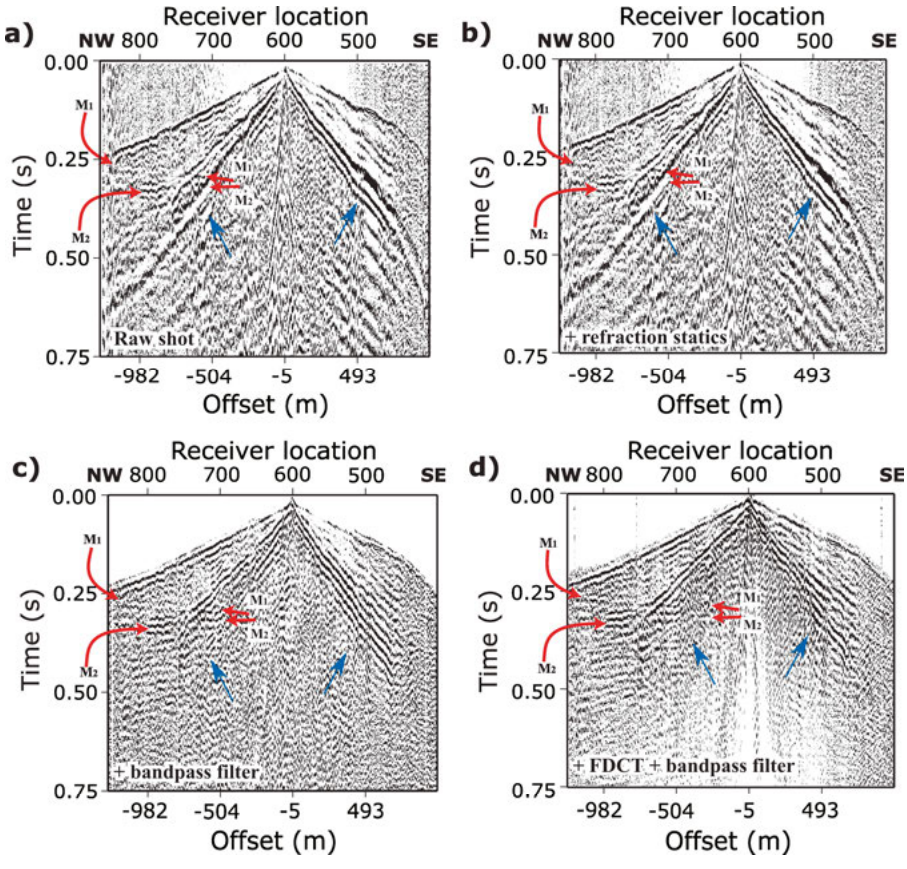

Figure 5.2. An example of shot gather form the dataset acquired in 2016, (a) raw gather showing some sign of reflections, which are likely generated from the mineralization; (b) after refraction static corrections; (c) after bandpass filter targeting low frequency component of the surface-waves marked with the blue arrows; (d) after curvelet denoising of the remaining surface-waves showing much more improved continuity of the reflections.

A 3D view of the migrated and time-to-depth converted section is shown in Figure 5.4. The known mineralization correlates well with reflections interpreted to be from the mineralization. Results in **Paper I** suggest that the mineralization extends beyond the known depth of 850 m from drilling works to about 1200 m. It additionally verifies the legacy borehole data that was used to suggest a depth extend to 850 m. This encourages planning of additional boreholes to validate continuation of the mineralization at depth and verify the nature of crosscutting reflections.

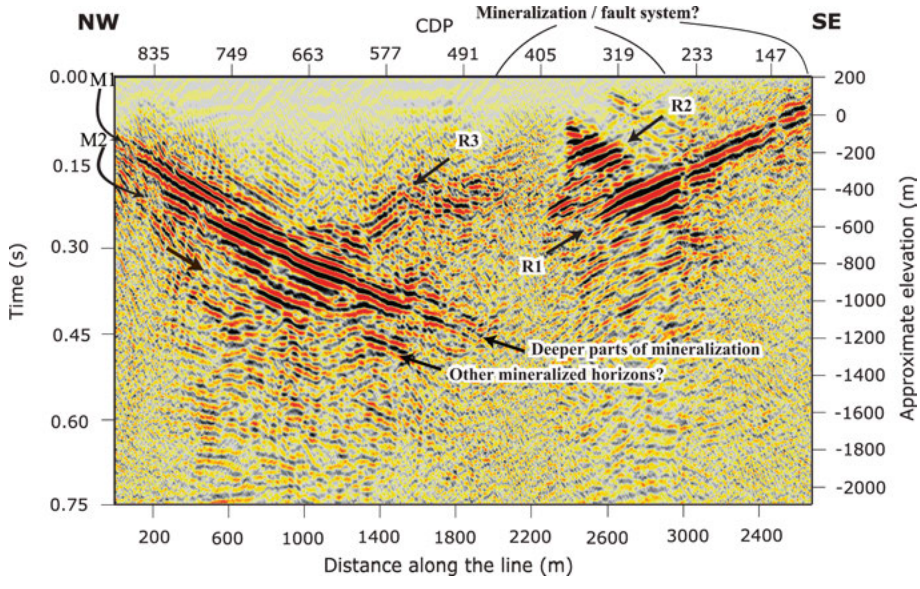

Figure 5.3. Unmigrated stacked section of the merged, 2015 and 2016, datasets showing the strong reflections M1 and M2 associated with iron-oxide mineralization. They show a continuous dip towards the SE, reaching a depth of approximately 1200 m. Another reflection underlying M2 can be a response of another mineralized horizon. The reflections showing a dipping towards the NW (R1, R2 and R3) can represent either fault structures or another set of mineralization connected to the M1 and M2 (forming a large syncline structure).

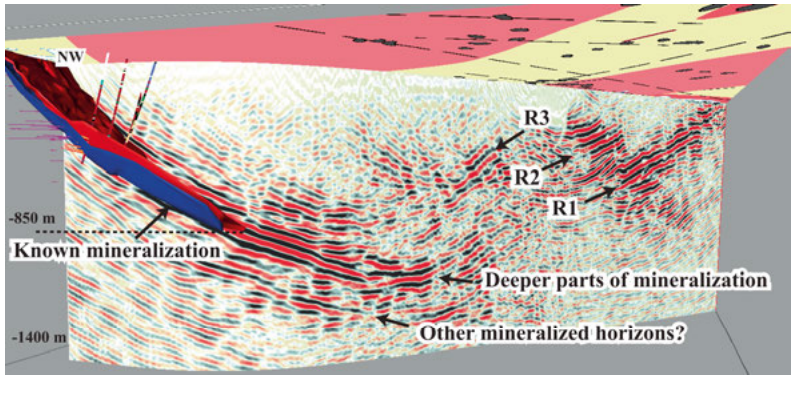

Figure 5.4. A 3D visualisation of the migrated and time-to-depth converted section of the merged 2015 and 2016 datasets. The known mineralization, blue and red surfaces, are visualised within the section and they correlate with the reflections interpreted to be from the mineralized horizons. The continuity of reflections implies possible existence of additional resources at depth. Reflections dipping opposite to the mineralization are not as continuous due to the low-fold coverage, hence their interpretation of being from fault systems is highly speculative from this study alone.

5.1.2 Conclusions

A workflow was developed for high-resolution imaging of iron-oxide mineralization by merging the two datasets collected along the same profile in two different field campaigns. Besides increasing the fold by merging the two datasets, special attention was given to the surface-waves attenuation using the curvelet denoising algorithm. The result suggests that the mineralization extends with depth about 350 m further and that there are possible additional underlying mineral-bearing horizons. The validation of these potential resources and structural interpretation should be continued with drilling campaigns and 3D seismic survey.

5.2 **Paper II:** Sparse 3D reflection seismic survey for deep-targeting iron oxide deposits and their host rocks, Ludvika Mines, Sweden

A sparse 3D reflection seismic survey was carried out in Blötberget mine, south-central Sweden. The main goal of the survey was to provide a high-resolution imaging of the iron-oxide deposits with depth and laterally, beyond its known dimensions. Additionally, the high-quality dataset allowed improved geologic structural interpretations of some of the main fault and fracture systems speculated in the previous 2D studies, as partly also described in **Paper I**.

5.2.1 Synopsis

The sparse 3D survey was designed as a follow up to the previous two 2D seismic campaigns (Malehmir et al., 2017; Markovic et al., 2020) to provide information on the extension of the iron-oxide mineralization laterally and with depth. The survey area of approximately 6 km^2, consisted of 9 receiver and 10 shot lines (Figure 5.5). Most of the shot points were generated at receiver locations and some additional shot lines were added to improve the data coverage for better illumination and fold. A 32 t vibro-truck was used as the seismic source, hence all possible roads with enough stability were used for shot points. An example of a raw shot gather is shown in Figure 5.6. Already in the raw shot gather, one can trace strong mineralization signature in almost all the receiver lines (Figure 5.6a). Combination of 2D and 3D statics improved the coherency of the reflections, whose quality was influenced by topography and the survey layout (Figure 5.6c). After applying bandpass filter and deconvolution, by suppression of the strong surface-waves, it was possible to observe three distinct reflections in one of the receiver lines, suggesting they might belong to different mineralization horizons (Figure 5.6d).

Example slices of the unmigrated stacked volume is shown in Figure 5.7. The inline slice shows several reflections dipping towards the south-west (M1 and M2), whose continuity stops with two sets of diffractions (D1 and D1) and a crosscutting reflection F1 dipping towards north-west (Figure 5.7b). In the crossline section, the same reflections are observed dipping towards the west with reflection F2 crosscutting them. Given the strong amplitude of the reflections M1 and M2 compared to others, they are interpreted as response from the mineralization. The two diffractions (D1 and D2) are appearing where reflection M1 and M2 stops, indicating that they are caused by the crosscutting reflection F1, which may suggest a fault structurer terminating M1 and M2.

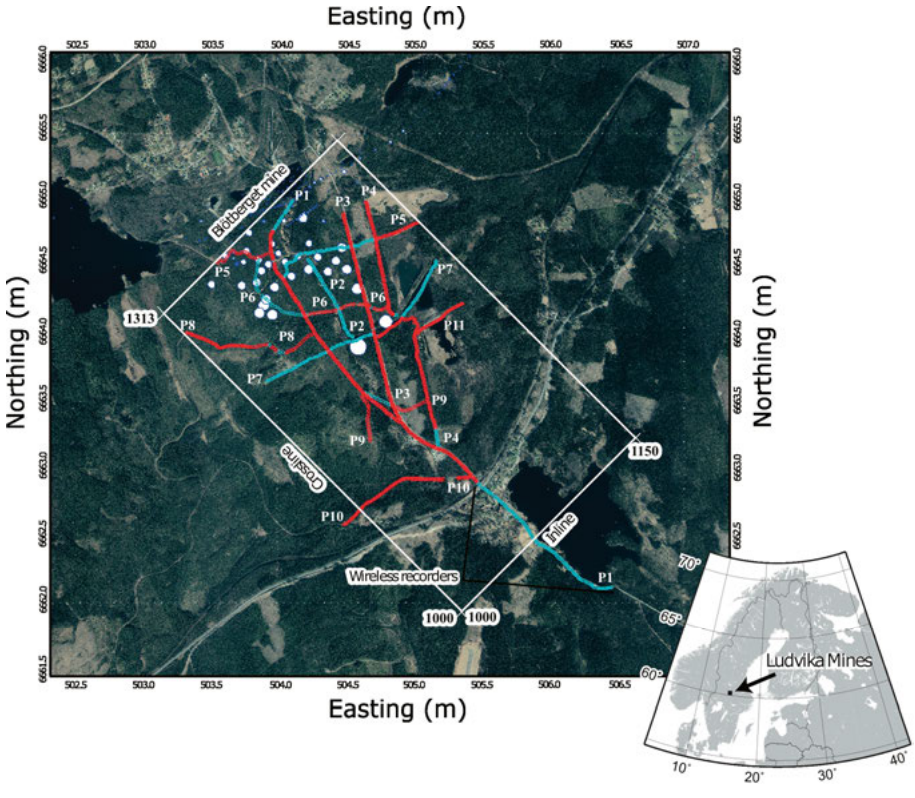

Figure 5.5. Aerial map of the sparse 3D reflection seismic survey. Red lines represent receiver locations, while the blue ones represent shot locations. Receiver spacing for most of the lines was set to 10 m, while some parts of the lines had 20 m spacing. Shot points were generated at every 10 m at every receiver location where possible and between receivers when the spacing was more than 20 m.

The 3D visualization of the migrated volume is shown in Figure 5.8. Within the volume one could identify several different reflections indicating different features, such as faults, folds, and mineralized horizons. The two crosscutting reflections (F1 and F3), dipping towards the west are interpreted as faults. Particularly with the support of a topography lineament, a strike for the faults was suggested in the NE-SW direction. The other short reflections within the volume were interpreted as possible fold structure (e.g., F2) and lithological contact (L1). The planes of the reflections were obtained by picking of the reflections from different inlines. These planes were visualized within the 3D volume and the known mineralization model to allow a better interpretation and representation of the results (Figure 5.8b).

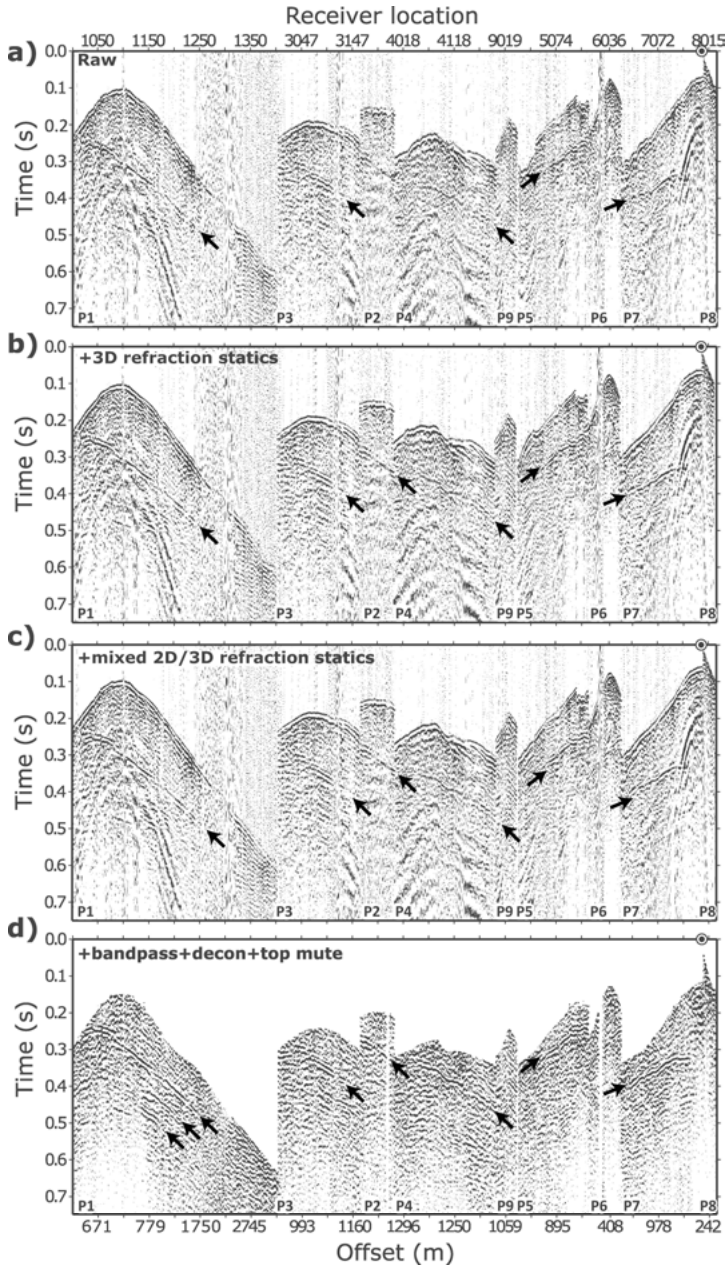

Figure 5.6. An example of (a) raw shot gather, (b) after only 3D refraction static corrections, (c) after a combination of 2D and 3D refraction static corrections (used further for processing), and (d) after denoised with a bandpass filter, gapped deconvolution, and a top mute. In comparison to only the 3D refraction static solution, the combination of the 2D and 3D statics improved the lines where topography and survey layout severely influenced the data quality. Black arrows point at the interpreted mineralization reflections.

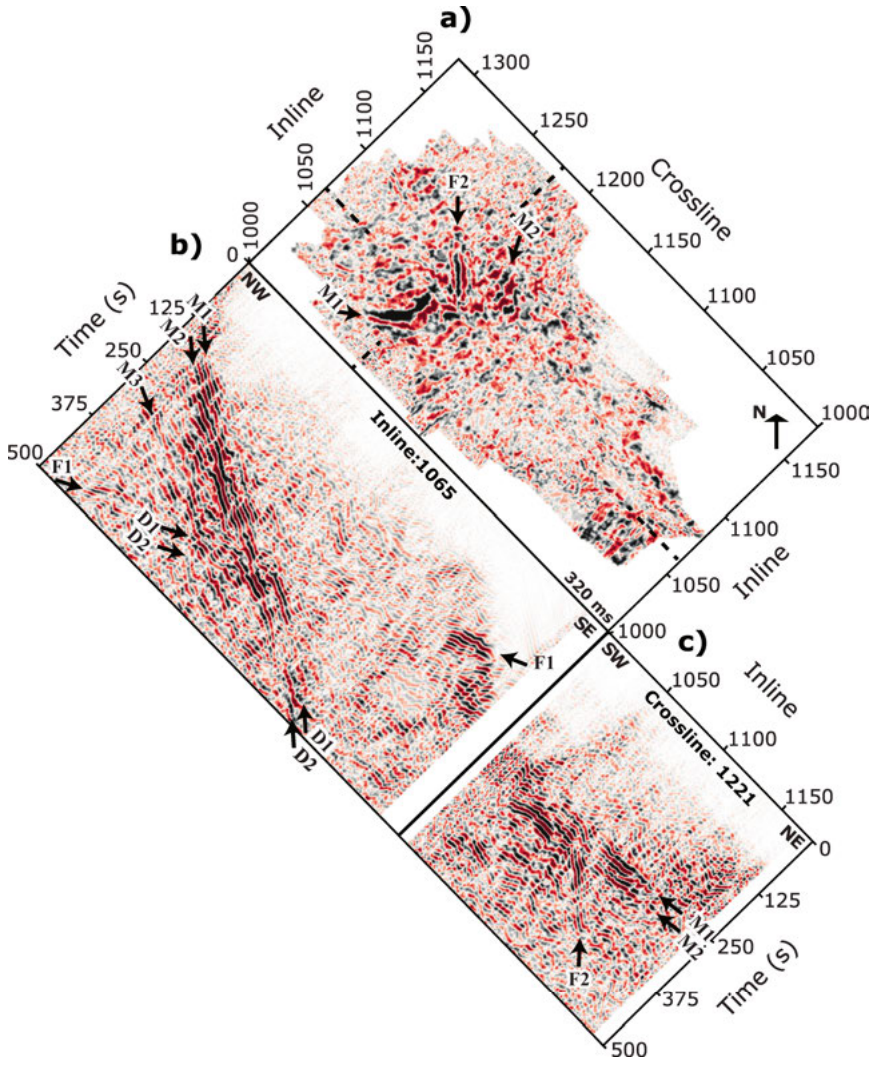

Figure 5.7. Series of slices extracted from the unmigrated stacked volume, (a) timeslice at 320 ms, (b) inline and (c) crossline. M1 and M2 are interpreted as reflections originated from the mineralization and M3 as possible additional resources. Diffractions D1 and D2 are interpreted to be associated with the fault F1, which possibly causes a sharp truncation of the mineralization at approximately 1200 m depth. The crossline section shows that M1 and M2 reflections are cut by F2.

Additionally, the high-amplitudes reflections corresponding to mineralization were extracted to produce a 3D extension of the resources. The additional resource model was added to the existing ore block model (Figure 5.8c) and considering that the reflections M1 and M2 extend down approximately 300 m further and laterally, an estimate of 10 Mt of potential additional resources was obtained providing a clear value the 3D seismic survey added in the study.

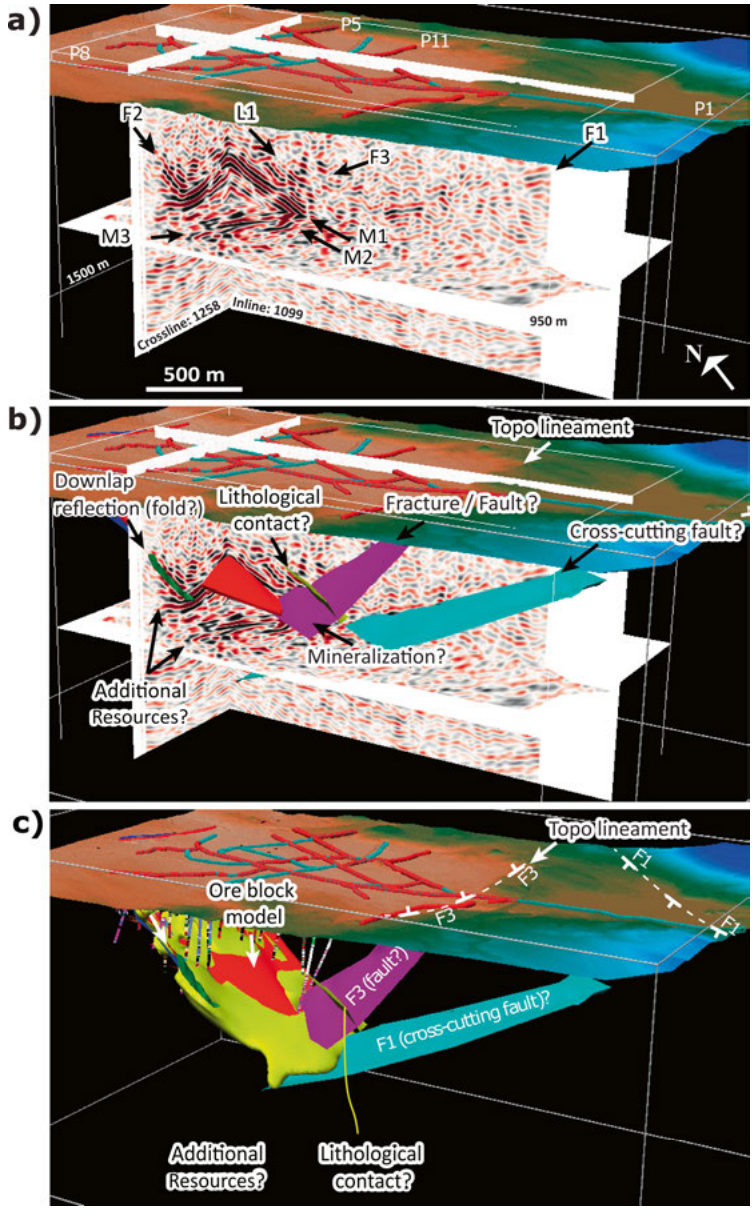

Figure 5.8. 3D visualisation of the migrated volume, (a) interpretation of the reflections from the mineralization (M1, M2, and possible M3), fault structures (F1 and F3) and short reflections indicating possible lithological contact (L1) and folding (F2); (b) generated surfaces of the interpreted features and (c) updated mineralization block model (yellow surface) from the 3D seismic survey.

5.2.2 Conclusions

A sparse 3D reflection seismic dataset was acquired in the Blötberget area to delineate lateral and depth extension of the known iron-oxide deposits. With certain processing steps, such as a combination of 3D and 2D refraction static solutions, it was possible to obtain an improved coherency of reflections in the shot gathers and eventual stacked volume. Later with standard processing workflow, several reflections corresponding to structural features, such as faults, folds and lithological contacts were imaged. A reflection package underlying the known mineralization was again observed indicating, and further confirming the results shown in **Paper I**, potential additional resources even at deeper levels. Overall, an estimate of 10 Mt additional resources was made from the 3D seismic survey from 300 m depth and lateral extents observed in the seismic volume. This should be verified and confirmed with future drilling campaigns. This study addresses the value of 3D seismic surveys for mineral exploration, among others, and can provide detailed structural interpretation that can be used for the future mine-planning works.

5.3 **Paper III:** Diffraction pattern recognition using deep semantic segmentation

A U-net algorithm was applied to synthetic seismic, real GPR and 3D hardrock seismic datasets for segmenting and recognition diffraction signal patterns. The synthetic seismic data were generated as proof-of-the concept and the first real case study was performed on a GPR section, which contained several strong diffraction signals, convenient for manual labelling. The 3D hardrock seismic dataset contained a strong diffraction signal generated from a VMS deposit (known as the deep zone). After passing it to the U-net algorithm, another, never labelled, incomplete diffraction signal, with similar amplitude strength was recognized alongside the already labelled diffraction from the VMS deposit. By revising the seismic volume and with additional modelling of diffraction traveltimes in 3D, the unlabelled diffraction suggested by the U-net algorithm was confirmed. This diffraction is generated outside the seismic volume and has similar character to the one of the VMS deposit (i.e., the deep zone), hence should be carefully studied and targeted. Overall, results showed a potential for diffraction pattern recognition even when only diffraction signal is segmented and for complex hardrock datasets with incomplete diffraction patterns.

5.3.1 Synopsis

Diffraction patterns have distinctive shape both in seismic and GPR data, hence it is suitable to target them using deep-learning algorithms that employ pattern recognition solutions (e.g., Dell et al., 2020; Dou et al., 2017; Lowney et al., 2021; Ma et al., 2020; Tschannen et al., 2020). **Paper III** studies the application of the U-net, supervised algorithm, developed by Ronneberger et al. (2015). As a proof-of-concept, over 150 zero-offset synthetic seismic sections were generated comprising over 20 point-diffractors and convolved with a 50-Hz Ricker wavelet using 10 m trace spacing. For the background velocity a constant 5900 m/s velocity was used as expected in one of the hardrock geological settings studied in this thesis. For the first example, contaminated sections with random noise in three levels: low, medium, and high-noise level (Figure 5.9) were used. All sections were labelled on the noise-free sections, which were used later for training. The input sections were broken into tiles to increase the number of the training images. For training, 80% of the data was used and the remaining 20% was used for testing and validation proposes. The prediction overlay showed that in the presence of the high-noise level, the diffraction pattern recognition would not provide continuous delineation and some pixels which correspond to the noise, could be mistaken as part of diffraction signals because they have the same pixel intensity (Figure 5.9f). For another synthetic seismic data example, the medium-noise level was kept and

randomly distributed coherent noise was added in different dipping angles (Figure 5.10). The prediction overlay showed that when diffraction tail overlaps with the dip of the coherent noise, the prediction would not consider that part as part of the signal (Figure 5.10e).

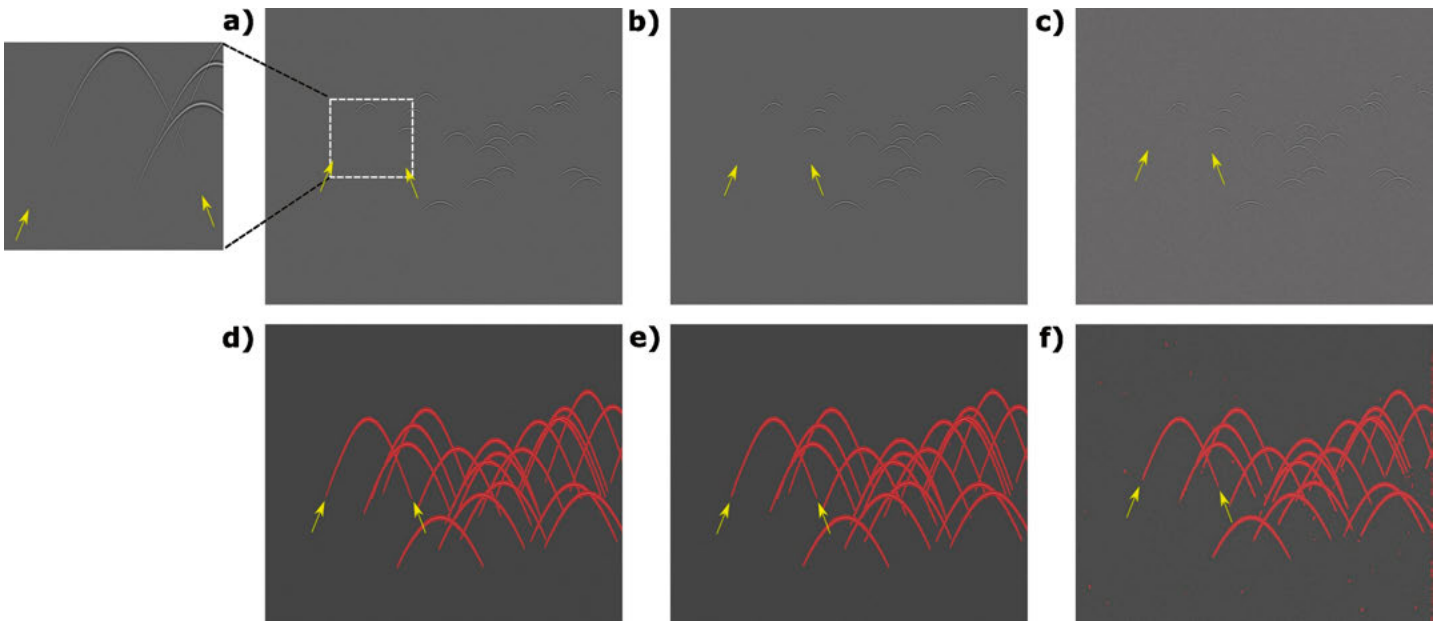

Figure 5.9. An example of a synthetic seismic section when contaminated with (a) low-noise level, (b) medium-noise level and (c) high-noise level. Diffraction signals are displayed within a close-up view as the section has large dimensions, hence the visibility of diffraction signals is not evident. (d-f) The recognized diffraction pattern, overlaid on top of the input sections, respectively. Yellow arrows point at the diffraction tails and in the case of the high-noise level, the diffraction tails are not completely recognizable since the signal is weaker.

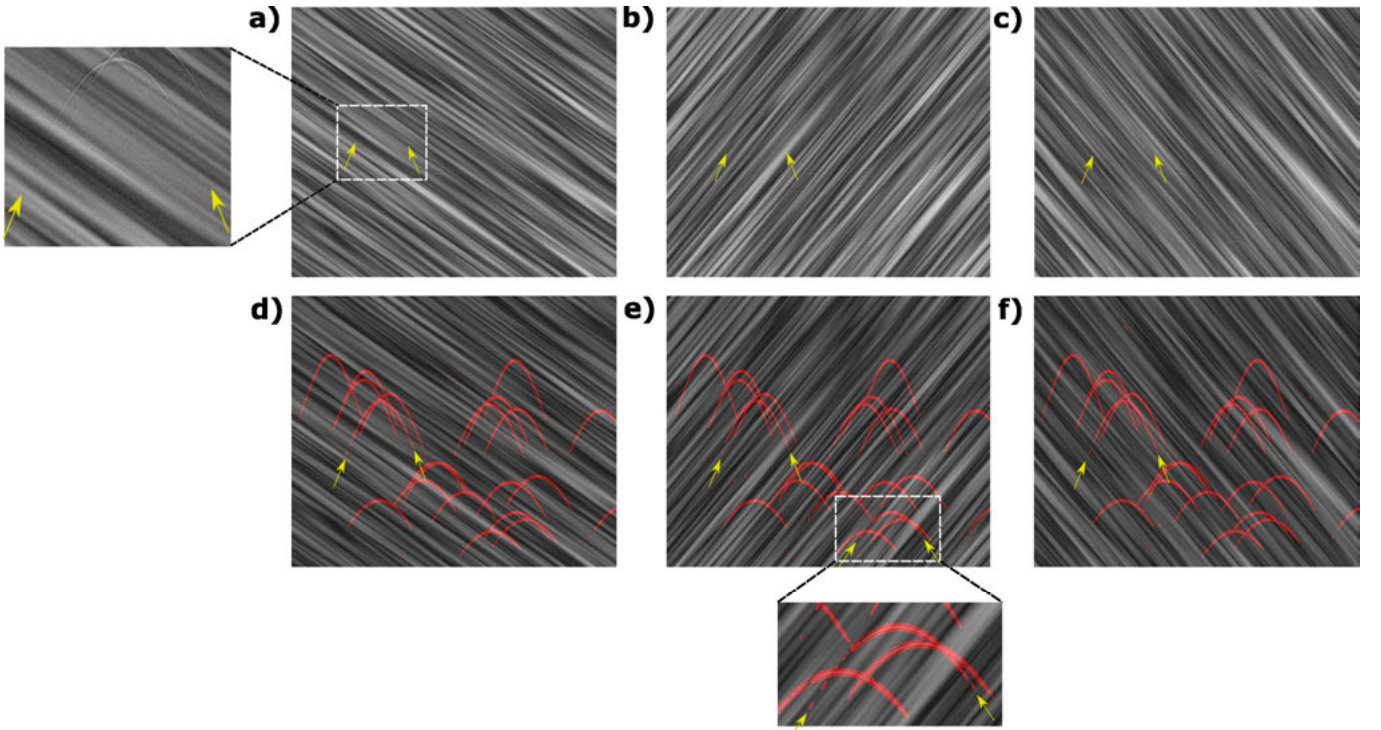

Figure 5.10. (a-c) An example of a validation set of different dipping noise angles and (d-f) corresponding prediction overlay. The close up of (a) shows clear positions of the diffraction signals. The close up of (e) shows how the prediction is not delineating the diffraction tails when there is an overlap with the same dipping angle of coherent noise. Yellow arrows point at the tails of some of the diffraction signals.

The first example of the real dataset was showcased through a GPR section (Figure 5.11a), and as such diffraction pattern recognition was expected to be successful even though the section contains strong clutter noise and reflections. The prediction results showed that some diffraction, which were missed during the labelling or not completely labelled, were recognized and delineated (Figure 5.11b,c). Also, some parts of the reflections were delineated as the pixel intensity is the same as pixels captured within the diffraction signal apex (Figure 5.11d).

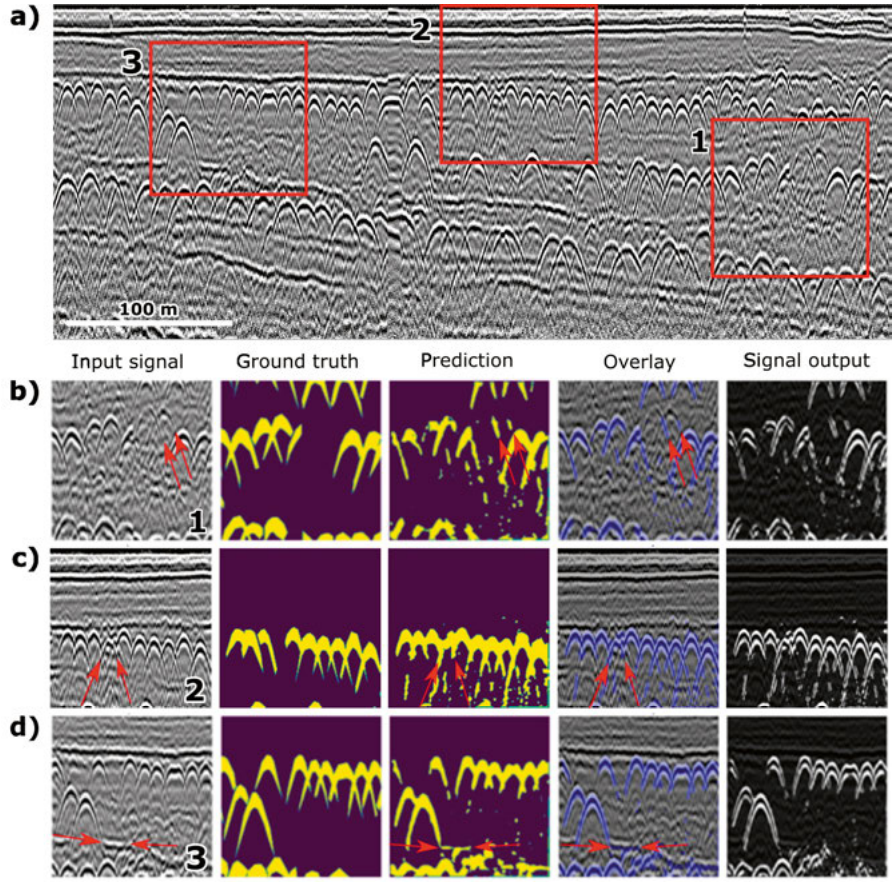

Figure 5.11. (a) A GPR section used for the diffraction pattern recognition. (b-d) Results of diffraction pattern recognition within the tiles of the section, used for the training. Red arrows point to the prediction results: (b) and (c) show that the algorithm recognizes the tails and apexes of several diffraction signals even though they were not initially labelled. (d) Prediction results showing the delineated part of the reflection signal, as the reflections have similar pixel intensities as the labelled diffraction.

Another real case study of using the U-net algorithm is represented on the historical Halfmile Lake 3D hardrock seismic dataset (Figure 5.12). The strong diffraction signal generated from the deep zone VMS body was annotated and all the inlines where the signal was pronounced were used; 80% for the training and 20% for testing and validation (Figure 5.12a). The prediction results showed, besides complete annotation of the known diffraction from the deep zone, an unexpected annotation of signal within some of the inlines (Figure 5.12b,c) at their edges. In previous studies, the annotated signal was interpreted as reflection, as the main objective then was to tackle the origin of the main diffraction from the deep zone (Malehmir and Bellefleur, 2009).

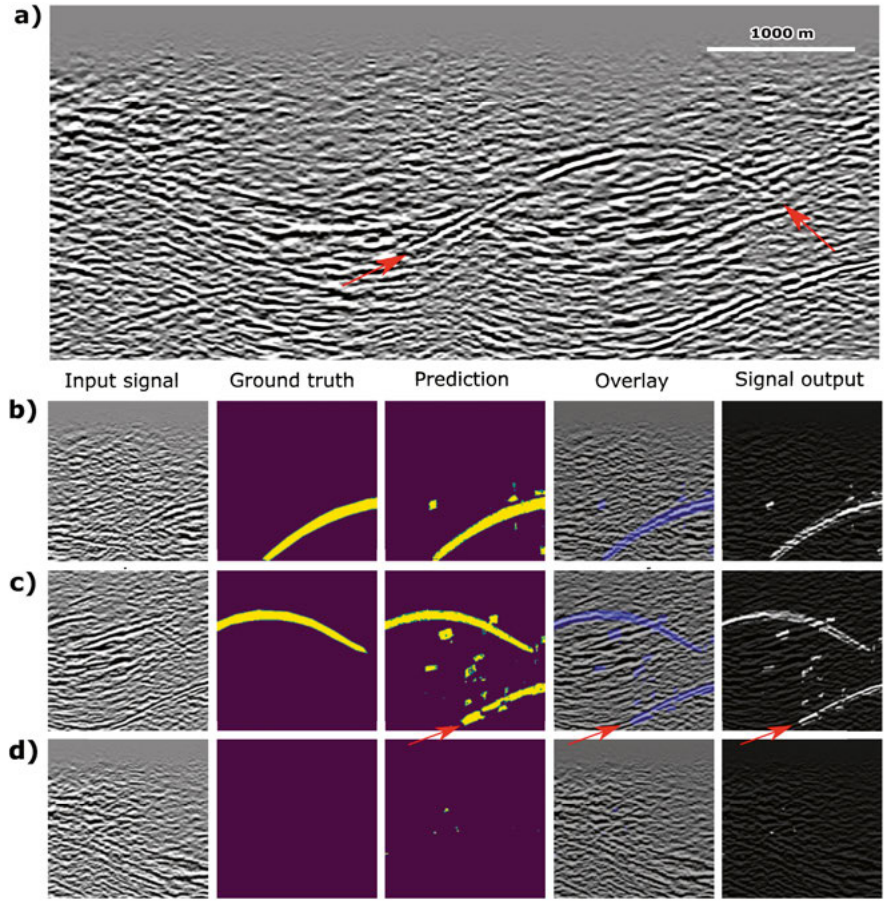

Figure 5.12. (a) One of the inlines used for the data training, and (b-d) examples of the prediction results of some of the tiles from randomly chosen inlines. (b) Completely delineated known diffraction from the deep zone. (c) Red arrows point to a never labelled yet predicted possible incomplete diffraction pattern. (d) When there was no label within the section, prediction did not provide significant scattered results validating the robustness of the workflow.

The annotation of possible incomplete diffraction led to additional investigations of the dataset to confirm the nature of the signal and its possible origin (Figure 5.13). Diffraction traveltime in 3D was formulated and calculated using a point diffraction formula; after plotting the results with the 3D seismic volume, the apex of another diffraction was found to be approximately about 500 m south-east away from the survey area and 1100 m deeper than the known deep zone. Such results and the nature of the newly confirmed diffraction signal can suggest potential discovery of another VMS deposits using supervised deep-learning solutions.

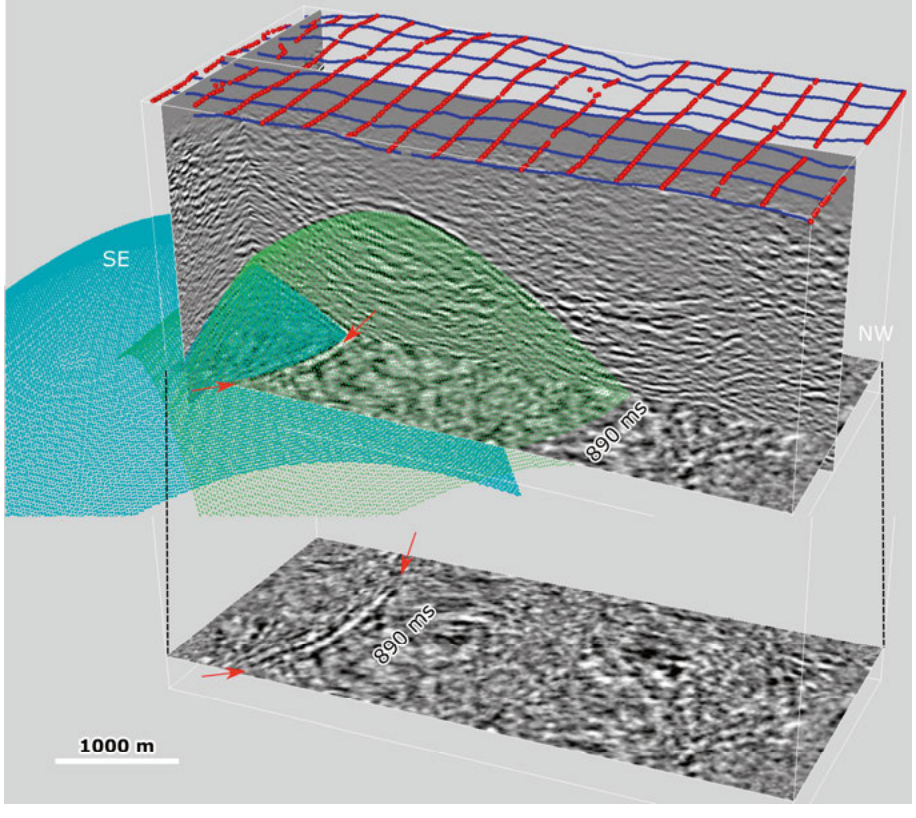

Figure 5.13. 3D view of the unmigrated seismic volume from the Halfmile Lake dataset and the extracted timeslice at 890 ms where the incomplete diffraction response was observed. Red arrows point to the diffraction signature on the timeslice. Diffraction hyperboloids were calculated and plotted within the volume for the known and the recognized incomplete diffraction. The tails of the incomplete diffraction match the signal observed in the crossline, inline and timeslice; this confirms that the U-net algorithm was able to recognize the diffraction pattern even when incomplete.

5.3.2 Conclusions

The U-net algorithm was used for diffraction pattern recognition on the synthetic seismic, real GPR and 3D hardrock seismic data. The synthetic data served as the-proof-of-concept and the algorithm was adapted for each dataset so that maximum optimization of the workflow could be achieved. The U-net algorithm could recognize diffraction patterns in both GPR and 3D hardrock seismic datasets, even if they were not labelled. Within the 3D dataset, the recognized pattern did not have a complete diffraction shape and with additional modelling of the diffraction traveltime in 3D, it was possible to confirm the algorithm finding. The additionally recognized diffraction pattern may be interpreted as a target hence additional investigations are suggested in the areas outside the current seismic volume. Further workflows can be improved with classification of other features within the section to minimize scattered prediction results and for multi-purpose pattern recognition.

5.4 **Paper IV:** Diffraction denoising using unsupervised learning technique

An autoencoder algorithm was applied to synthetic seismic, real GPR and 3D hardrock seismic datasets this time for diffraction signal denoising both section images as well as plane views or specifically timeslice sections. Additional image processing techniques were coupled within the autoencoder to provide sharper representation of the autoencoder solution and possibilities for automatic targeting of diffraction signals. The aim of this study was to test and develop the autoencoder workflow primarily for hardrock seismic datasets and targeting deposits at depth.

5.4.1 Synopsis

Unsupervised deep-learning algorithms are widely used in processing and particularly interpretation of seismic and GPR data (Bauer et al., 2022; Dell et al., 2020; Puzyrev et al., 2022). Image-based unsupervised algorithms, such as autoencoder, can provide fast and reliable solutions with no requirement for manual labelling, when enough training data is provided. In **Paper IV**, the possibilities of implementing the autoencoder algorithm to denoise diffractions when poor signal-to-noise ratio is present were explored. First, the algorithm was tested on synthetic seismic data contaminated with both random and coherent noise, masking the diffraction signals, used for the study in Markovic et al. (2022a) (**Paper III)**. Sections were broken into tiles and each tile was used as a separate image for model training (Figure 5.14a). The predicted noise of one of the tiles is shown in Figure 5.18b. Most of the coherent events were successfully attenuated, in particular the ones with strongest amplitude, which were completely masking some parts of the diffraction signals (Figure 5.14c). To provide sharper representation of diffraction signals, including the removal of the remaining coherent events, the Hough transform for the straight-line detection (Figure 5.14c-e) were used. Considering that binary representations are required for the Hough transform containing remaining both random and coherent noise, the pixel edge detection was applied to target and delineate only strongest and most continuous events, in this case diffraction. The pixel edge detection removed most unwanted data, leaving besides diffraction, two strong coherent events (Figure 5.14 g). At this stage, it was straightforward to target and isolate these coherent events with linear Hough transform (Figure 5.14h,i).

As for the real data, autoencoder workflow was first applied to GPR sections, which contained strong diffraction signals. The first example shown in Figure 5.15 suggests that if a signal has a strong amplitude (pixel intensity), part of the predicted noise will include those amplitudes, while as in the case

of a weak signal, the predicted noise would not include pixels from the diffraction tails. Another GPR data example, collected along a concrete bridge deck, containing several diffraction signals of the same shape were targeted as it was convenient for the data training (Figure 5.16). The predicted noise result (Figure 5.16b) shows continuous reflections with removed diffraction instead even when the signal was weaker. The autoencoder solution shows separated diffraction (Figure 5.16c), and overall potential of using the autoencoder workflows when diffraction is treated either as a noise or signal.

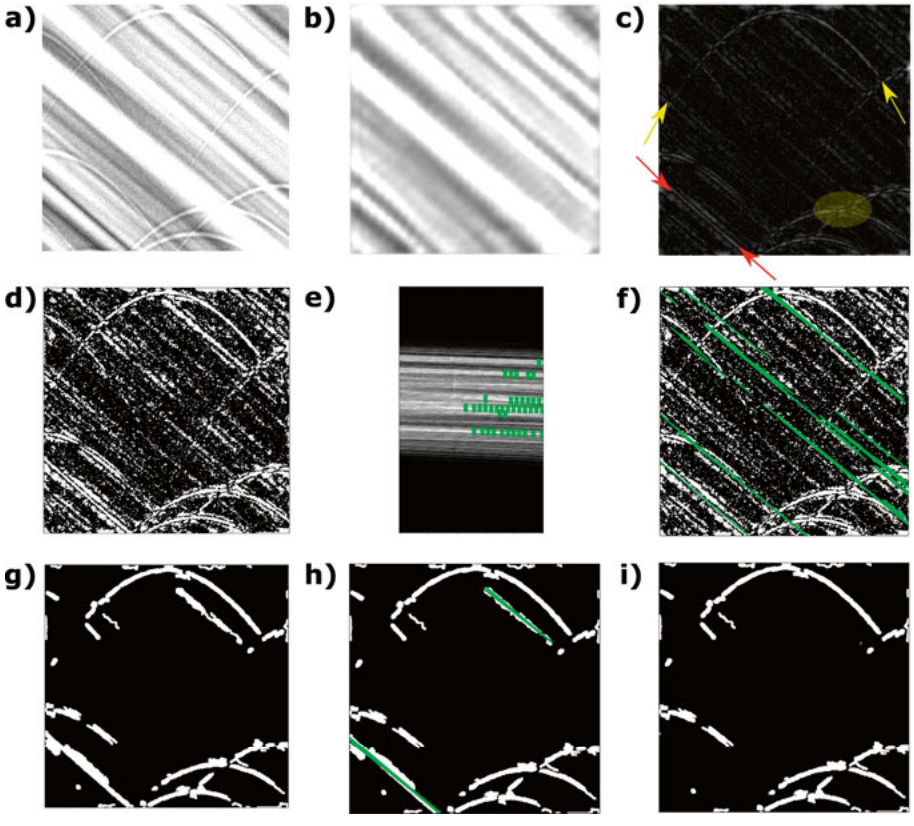

Figure 5.14. An example of (a) one of the tiles within the synthetic seismic section used as the input tile, (b) the predicted noise and (c) autoencoder solution. Yellow arrows point to the tails of one of the diffraction signals. The yellow-shaded area in (c) marks successfully denoised part of the diffraction, where the noise had the strongest amplitude (pixel intensity). Red arrows point to coherent noise, whose structure appears as part of the diffraction. (d-f) Application of the Hough transform on the autoencoder solution for the straight-line detection. (g) Pixel edge detection of the autoencoder solution for mainly random noise removal and (h,i) detection and removal of the remained coherent events.

The last example of the autoencoder application was on a 3D hardrock seismic dataset collected over a VMS deposit (Matagami) in Canada. The first attempt

of employing the autoencoder denoising workflow was on inline sections of the dataset, which contain diffraction signals and one of them is from the known Bell Allard deposit (Adam, 1997). To increase signal-to noise ratio and prevent the autoencoder to correlate both reflections and diffractions as relevant for denoising, for data training we applied additional filters to the dataset such as bandpass, FK filters and F-XY deconvolution (Figure 5.17). Even the diffraction was enhanced, the autoencoder algorithm required a different strategy for diffraction denoising because of the remaining reflections, which could not be attenuated with only post-stack filters.

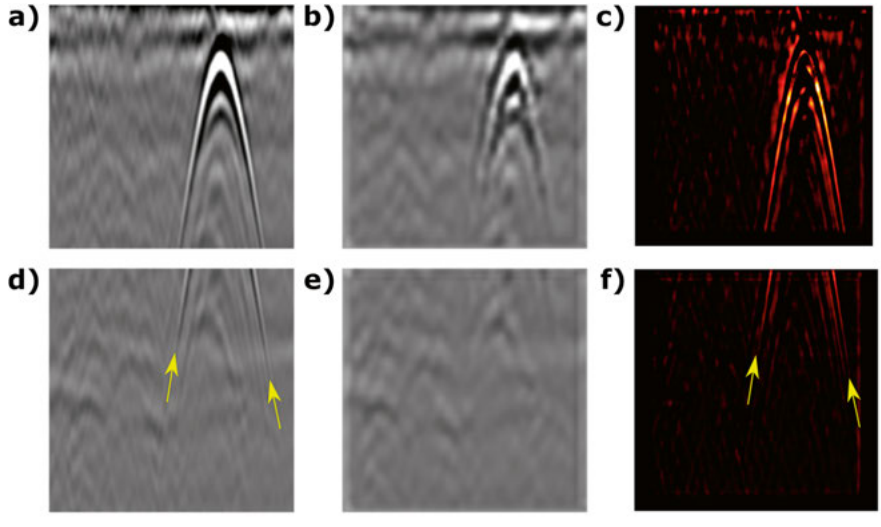

Figure 5.15. An example of one of (a) the input tiles of the GPR section, (b) noise prediction and (c) autoencoder denoised diffraction. (d) Another example of the tile that contains weak signature of diffraction tails, (e) the predicted noise, and (f) autoencoder solution. Yellow arrows point to the tails of the diffraction, which are successfully kept by the autoencoder algorithm.

Instead of applying the algorithm on the inlines, because the diffraction has a distinct circular signature in timeslice in comparison to reflections, it was decided to use it in this domain (Figure 5.18). Timeslices were extracted where strong diffraction signature of the Bell Allard deposit was observed, and post-stack filtered timeslices were used for the training (Figure 5.18b) and autoencoder denoising was performed on the original, input timeslices. The autoencoder in this case strongly suppressed the noise and the diffraction signature was not visible to a human eye (Figure 5.18c). Therefore, pixel edge detection was applied to further delineate the diffraction circle in binary view for original, filtered and autoencoder denoised timeslices (Figure 5.18d-f).

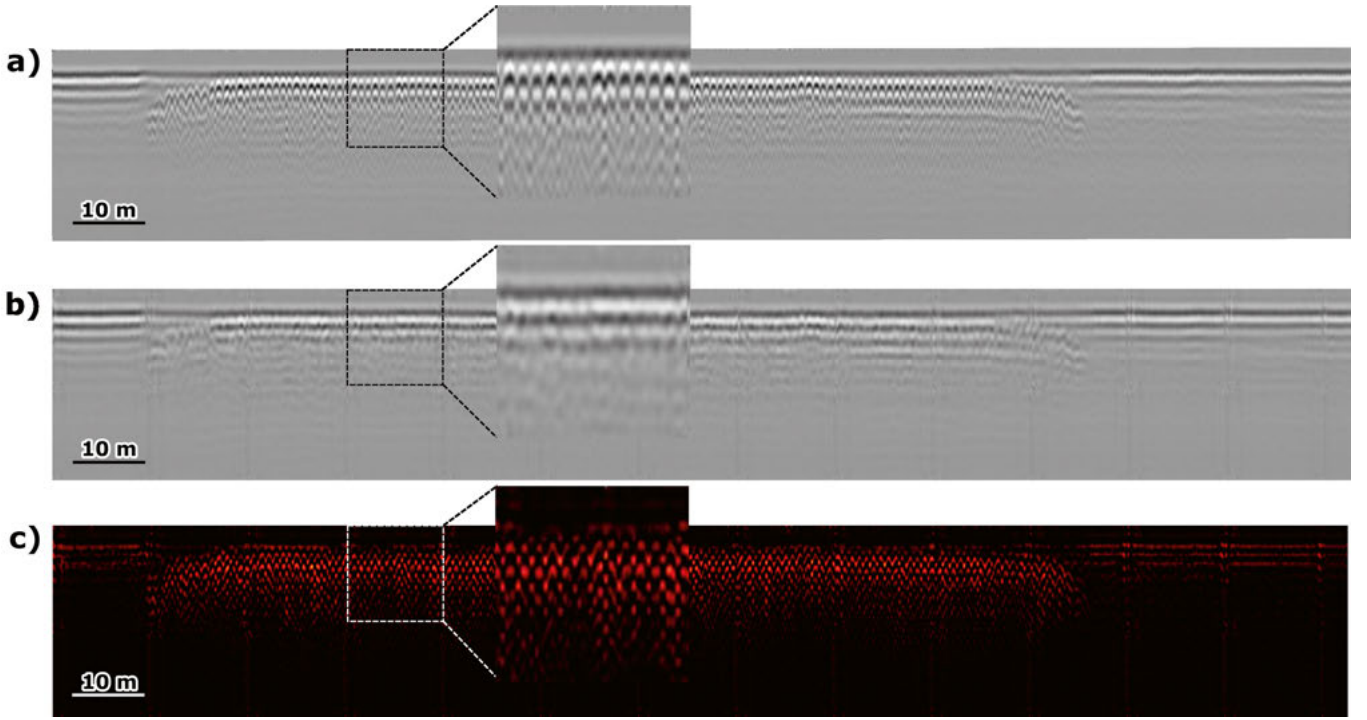

Figure 5.16. The reconstructed GPR section of (a) the input tiles, (b) predicted noise and (c) autoencoder denoised solution. Close-up views indicate the position of one of the tiles. Predicted noise in (b) and autoencoder denoised section in (c) suggest that the autoencoder algorithm can be successful in both cases i.e. when diffraction is treated as a noise or as a signal.

To make a comparison between the three timeslices, the images were levelled to the same pixel coefficient. The autoencoder-denoised timeslice although not displaying a continuous half-circle, it did not show any of reflections compared to the original and post-stack filtered timeslice. Following the experiment of using the Hough transform for the straight-line detection for removal of the coherent events, this time the Hough transform was used for the detection of circular features. The results of detected circles are shown in Figure 5.18d-f.

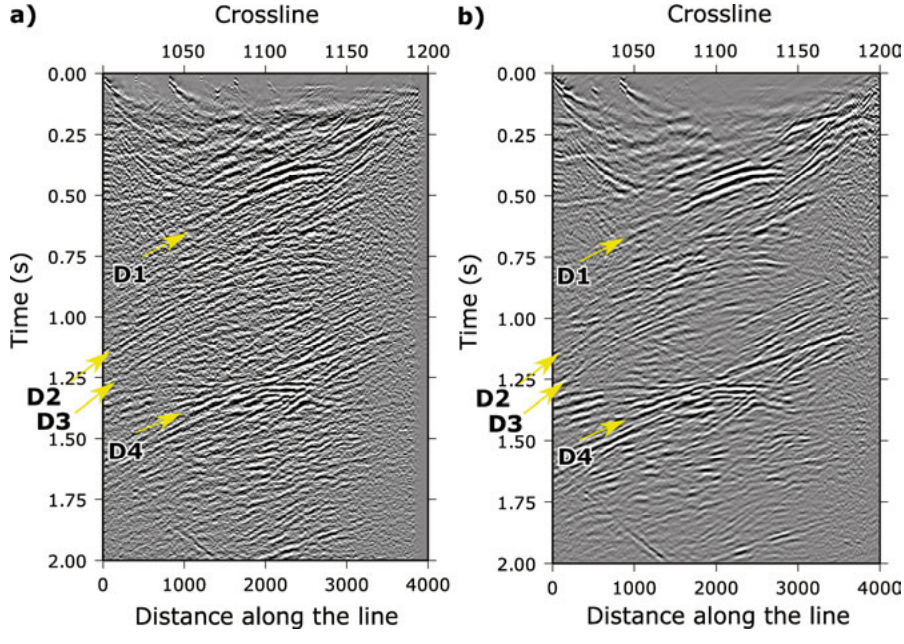

Figure 5.17. (a) One of the inlines from the 3D hardrock seismic datasets and (b) same inline, post-stack denoised using a bandpass filter, FK filter and F-XY deconvolution. Yellow arrows point at some of the diffraction signals at different times. Diffraction marked as D1 represents response from the known Bell Allard VMS deposit.

As Hough transform performs on a voting principle, narrowing down the circle candidates for the given radius, the input parameters were kept the same for all the edge detected timeslices. The autoencoder solution provided a single circle choice (Figure 5.18f), suggesting that the Hough transform coupled with autoencoder solution can lead to improved automatic detection of diffraction circles in 3D datasets. Even more, in this case, when diffraction response is associated with the deposit and when data contain many other similar diffraction responses, development of such a workflow can help discovery and targeting of potential deposits at depth.

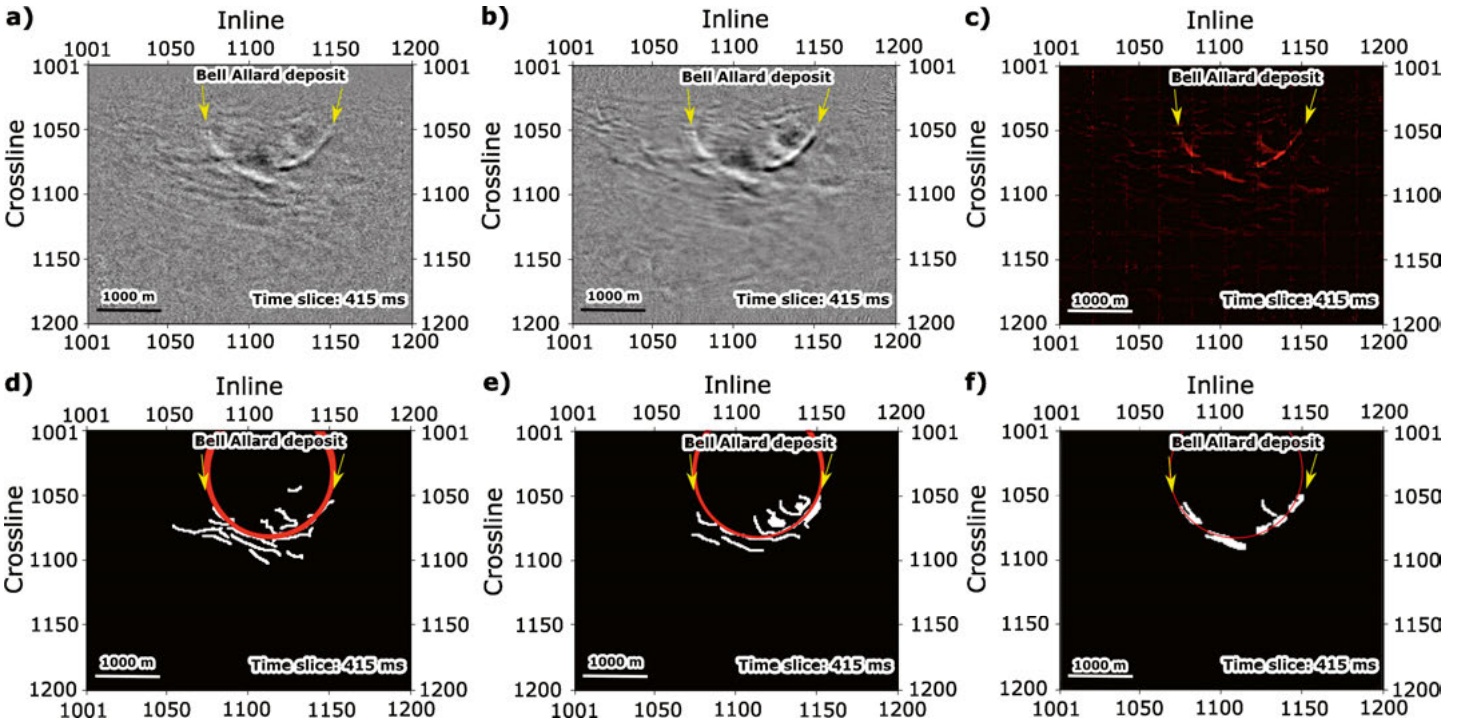

Figure 5.18. The timeslice example of the 3D Matagami hardrock seismic dataset, which contains the strong diffraction signature from the known Bell Allard VMS deposit of (a) original data, (b) when bandpass, FK-filter and F-XY deconvolution applied, and (c) the autoencoder denoised original timeslice. (d-f) The edge detected timeslice of the original, filtered and autoencoder denoised data, respectively. Yellow arrows point at the diffraction half-circle. The red circles represent automatically detected circles using Hough transform.

5.4.2 Conclusions

To denoise diffraction signal, autoencoder algorithm was applied on the synthetic seismic and real GPR and 3D hardrock seismic datasets. The best performance of the autoencoder was showcased on the GPR data, given that the GPR diffraction has stronger amplitude and repeated and correlated signal, which is convenient for the autoencoder to recognize as the most important information hence retaining in the denoised image. The complex cases of the synthetic seismic and real 3D hardrock seismic datasets needed additional image processing works to deliver sharper representation of the autoencoder solutions. Pixel edge detection and Hough transform was used in this case to eliminate remaining noise and automatic delineation not only of the noise, but also the diffraction signal on the timeslice. All examples used in this study illustrate wide application of the autoencoder for diffraction denoising, and for hardrock seismic datasets, where the signal can be response of a reasonable size deposit. The proposed workflow in this study initially suggests a potential for the combination of unsupervised and semi-automatic algorithms for diffraction denoising when a low signal-to-noise ratio is present.

6 Conclusions

This thesis illustrates various possibilities to maximize the value and effectiveness of seismic data and surveys for deep targeting of mineral deposits through tailored acquisition setups, and novel processing and interpretation workflows. The first two papers tackle high-resolution reflection seismic imaging in 2D and 3D for direct targeting of iron-oxide deposits at a site in central Sweden. The other two papers employ deep-learning algorithms to delineate diffraction patterns from VMS deposits at two sites in Canada.

For the study in **Paper I**, the aim was to obtain high-resolution 2D data by merging two datasets acquired along the same profile in two different field campaigns. The first field campaign was conducted as an experiment to validate a state-of-the-art landstreamer system instrument developed for urban applications, and whether it was suitable for deep-targeting of iron-oxide deposits and open-up possibilities for future surveys. The second field campaign was carried out using shorter length compared to the first one. By analyzing both datasets, it was decided that a higher fold and longer 2D profile can be obtained by merging of the two datasets, which made it possible to image deeper parts of the mineralization and speculate on potential crosscutting structures.

The follow-up sparse 3D reflection seismic survey (**Paper II**) was planned based on the 2D surveys. Although the survey was designed in a sparse manner due to environmental and budget constraints, it was possible to image the deposits laterally and at depth. The 3D volume provided not only an estimation of additional potential resources, but also the possibility to infer fault planes and fold structures associated with the deposits. All these were not possible using only 2D surveys.

In the second part of the thesis (**Papers III** and **IV**) the value of diffraction response of VMS deposits as opposed to the reflections studied in **Papers I** and **II** was shown. The diffraction signatures of the two VMS deposits and an additional one from an unknown affinity were studied using the deep-learning algorithm workflows. Both supervised and unsupervised deep-learning solutions were employed for diffraction pattern recognition and denoising within the 3D seismic datasets. The delineation of an incomplete diffraction response with an origin estimated to be outside of the seismic volume was the highlight of these workflows since it may imply new targets adjacent to the current seismic volume reinvigorating the dataset for future exploration works.

The presented studies within this thesis encourage expanding seismic surveys at all the three study sites, especially with additional drilling works to verify possible targets and interpretations generated in this PhD work. Application of the developed workflows on similar datasets and geological settings would help to improve and adapt the workflows and their ability to provide new targets with higher efficiency and fidelity.

7 Future research possibilities

The seismic studies of this thesis at the historical Blötberget mining site in Sweden are among many others carried out within the scope of the Smart Exploration™ project for testing innovative exploration technologies and methodological solutions (Balestrini et al., 2020; Hloušek et al., 2022; Malehmir et al., 2021; Maries et al., 2020; Markovic et al., 2020; Papadopoulou et al., 2020; Singh et al., 2022). The site has endeavored to be reopened in the near future, hence additional studies may be necessary to facilitate this process and help the mine to effectively sustain for a longer period.

In the scope of the studies in my PhD thesis, the sparse 3D dataset was also used for first-break traveltime tomography. Results showed a sharp change to low velocities at the position of a historical tailing in the eastern part of the survey area. Also, extracted from the 3D survey, 2D profiles were extracted with a focus on improving the mineralization image under the mine tailings in order to characterize its thickness and geomechanical properties. The tailing was estimated to be approximately 50 m thick having reasonable resources to be included for mineral reprocessing and extraction (Alofe, 2021). These two studies combined can therefore suggest planning of another smaller-scale high-resolution 3D seismic survey over the tailing to better characterize its 3D geometry and stability for future mine-planning purposes. It can benefit from modern sensing technologies such as small nodal arrays and fiber optic sensing solutions, also multi-component surveys.

Smart Exploration™ project benefited from strong industry-research collaborations, allowing to develop and execute different experiments for efficient mineral exploration. It led to new initiatives and research possibilities via other R&D projects. The most recent experiment at the site and along the same profile as the first article, included passive- and active-source surface and borehole fiber-optic (or DAS) data acquisition, testing of high CDP fold (approximately 250) broadband (MEMS) receivers in conjunction with broadband sources (2-200 Hz sweeps) and exploring the possibility of recording wave-mode conversion from the mineralization via 3C data recording. Within the same study, two new profiles, 3 km northeast of the site were acquired for imaging possible extension of the mineralization and key geological structures. The new two profiles benefited, in their planning, also from recent airborne (Malehmir et al., 2020) and detailed UAV magnetic surveys (Bastani and Joahansson, 2022).

The applied deep-learning workflows for diffraction recognition and modelling the diffraction traveltime in 3D should be developed further for understanding the diffraction origins of those found in the Blötberget sparse 3D dataset. This would require building of a global training model for diffraction pattern recognition and possible application of the autoencoder algorithm in 3D (e.g., Ma et al., 2022; Zhu et al., 2014), meaning diffraction patterns can possibly be recognized directly within the volume. This initiative could encourage re-examination of the legacy data collected at different hardrock settings for mineral exploration and possible delineation of new targets. The Blötberget dataset contained several other diffraction signals that appeared to have a general trend within a concave (fold) structure than the one interpreted from faults (Figure 7.1). An attempt was made to find the trend if this means a fold axis (crest) from a tight fold, however, it failed due to the complexity of the diffraction signals and the quality of the 3D seismic volume being a rather narrow azimuth dataset. Solving this enigmatic diffraction pattern, if from a tight fold, can lead to new possibilities about the depth and lateral continuation of the deposits at the Blötberget site and allowing a super-resolution interpretation of the 3D data.

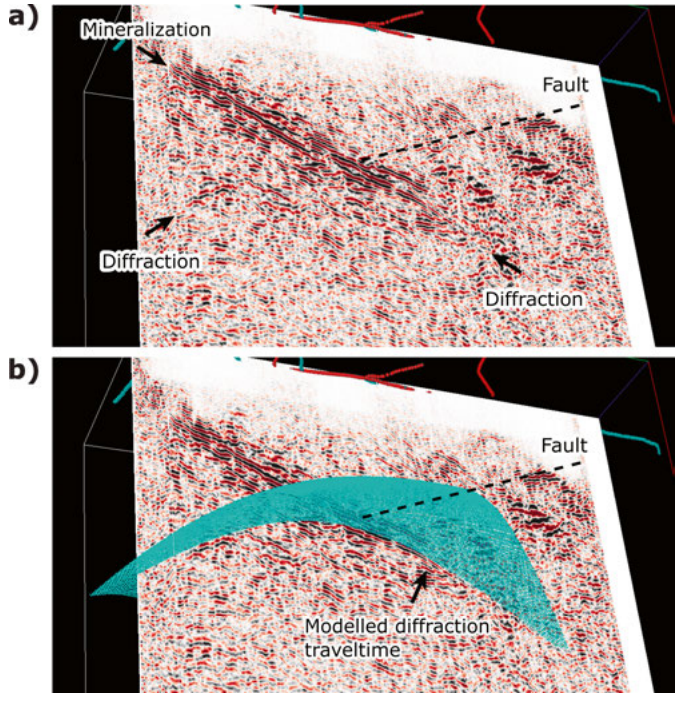

Figure 7.1. (a) One of the diffraction signals noted within the Blötberget 3D seismic dataset interpreted to be generated by a fault truncating the mineralization and labelled with arrows. (b) The diffraction signal modelled (blue hyperboloid surface) as a point diffractor within the volume.

8 Summary in Swedish

Geofysiska metoder i allmänhet, och reflektionsseismik i synnerhet, blir en allt viktigare metod för mineral- och malmprospektering, särskilt för fyndigheter på stora djup. Denna avhandling ingår i Smart Exploration™-projektet, ett forsknings- och innovationsprogram för mineralprospektering, som finansierades av EU-kommissionen mellan 2018–2020.
Avhandlingen bidrar till utveckling och tillämpning av seismiska metoder i kristallint berg genom förbättrad avbildning och avgränsning av mineralfyndigheter, som kan komma att bli föremål för framtida prospektering. Syftet med denna avhandling är att förbättra kvalitet och kostnadseffektivitet av insamlade data vid reflektionsseismiska undersökningar, och därigenom maximera dess värde. Målen har uppnåtts genom att utveckla skräddarsydd datainsamling vid fältmätningar och nya arbetsflöden för bearbetning och tolkning. De lärdomar och experiment som presenteras är användbara för akademi och industri och bidrar till råvarusäkerhet och hållbarhet.
Denna sammanläggningsavhandling består av fyra artiklar (3 publicerade, 1 under granskning). De två första artiklarna presenterar nya arbetsflöden för kartläggning av järnoxidmineraliseringar vid Blötbergets gruva i Mellansverige med hjälp av högupplöst reflektionsseismik. De andra två artiklarna använder djupinlärningsalgoritmer för att beskriva diffraktionsmönster från vulkanogena massiva sulfid-avlagringar (VMS) i gruvdistrikten Halfmile Lake och Matagami i Kanada.

I **Artikel I** kombineras mätdata från två nära vinkelrätt strykande 2D-reflektionsseismik profiler i området för att uppnå tillräcklig datatäckning för att avbilda järnoxidmineraliseringen på djupet. Dominanta ytvågor dämpades med snabba diskreta kurvformade transformationer, vilket möjliggör en förbättrad avbildning av mineraliseringen. Resultaten visar att de starka reflektorerna från den kända fyndigheten fortsätter mot djupet, vilket tyder på en möjlig förlängning mot djupet av den kända mineraliseringen med cirka 350–400 m. Resultaten från **Artikel I** användes vid planeringen av den glesa 3D-undersökning i **Artikel II**. Trots en begränsad azimutförskjutnings-täckning och några möjliga mätartefakter från datainsamlingen, har mineraliseringen och dess förlängning kunnat avbildats, både i sidled och med djupet. Nya reflektorer har observerats och nya geologiska strukturer har tolkats, vilka ökar kunskapen om fyndighetens tredimensionella geometri och hur de geologiska strukturerna kontrollerar dess form.

I avhandlingens andra del (**Artiklar III och IV**) har diffraktionssignaturerna för de två kanadensiska VMS-fyndigheterna studerats genom att tillämpa två typer av djupinlärningsalgoritmer som del av arbetsflödet. I **Artikel III** tillämpas en övervakad djupinlärningsalgoritm, vilken resulterat i att flera nya men ofullständiga diffraktionssignaturer har observerats. Dessa kan vara nya möjliga mål för framtida prospektering. I **Artikel IV** tillämpas en oövervakad algoritm för djupinlärning, i kombination med ytterligare bildbehandlingsverktyg som en del av arbetsflödena. Dessa tillägg till arbetsflödena resulterar i förbättrad avgränsning av diffraktionssignaturerna, vilket i sin tur signalerar att de kan användas för att avgränsa och detektera diffraktionssignaler för ett tidsintervall, åtminstone för signaler med en cirkulär form.

Resultaten från denna avhandling visar att utökad användning av seismiska fältmätningar och tillämpning av de nya arbetsflödena gynnar kvaliteten av framtida undersökningar vid de tre studieplatserna i Sverige och Kanada, särskilt i kombination med och för planering av prospekteringsborrning. Tillämpning av de utvecklade arbetsflödena på liknande fältdata kommer att förbättra resultatens kvalitet, stödja en tidseffektiv datainsamling och analys, vilket kommer att förbättra identifiering av nya fyndigheter i liknande geologiska miljöer, det vill säga andra järnoxid- och VMS-mineraliseringar i kristallint berg.

Acknowledgements

To you dad, it all began with you. I know you will never be able to read this, but I must speak my heart somehow. I have always admired your knowledge about anything someone could mention. You always had an answer. You always had a solution, either theoretical or practical. You are the one who showed me what is the life in academia like and how science and positive attitude can bring you anywhere. You took me to the biggest conference I have been and when I saw all the people hugging you and looking at you full of joy, it was clear to me that day who I want to become. And I am there, following the path with you in my heart all the time. I hope you are proud of me!

My geoscience journey started exactly 10 years ago. I am grateful for the knowledge I obtained from my professors at the University of Belgrade and even more, I appreciate the opportunities I got outside of the university, which basically brought me to Uppsala. Being part of Uppsala's Applied Geophysics group was my dream since I was at my second year of Bachelor studies (2013/14); was it a destiny or not, I made it here! In June 2015, I met three important professors who would be crucial for my development as a young professional: Snezana Komatina, Milovan Urosevic and Alireza Malehmir.

Thank you, professor Snezana, your commitment to your students is so admirable and you are more than a professor to me, my geophysics mother. Thanks to you, and your efforts to involve students into international projects, which opened a great opportunity for me to develop my communication skills among others. And thank you Milovan (I know you don't like it when I call you professor), for hosting me at your exploration geophysics department at Curtin University. It was a great experience for me, and I have learned a lot from you.

Alireza, thank you for believing in me. I said this sentence many times, but I am enormously grateful I had you as my supervisor. You always gave me space to learn, but I am most grateful that you let me develop my creative and critical thinking! Thank you as well for supporting me with all side activities within EAGE, SEG, AGES and BGS communities, and making your students/team popular as you are. Besides being a great supervisor, I am proud I can call you my friend after all these years. I hope our paths will cross many times in our lives and that you will be proud of me every time we meet. Moreover, I should not forget to thank you for all those extreme fieldworks, or rather I should call them fat camps! I lost many kilos, but I gained a lot of practical knowledge, a win-win situation I must admit.

I want to thank all my colleagues (Ruth, Emil, Mehrdad, Peter, Greg, Magnus, Möhsen, Paula, Thorben, Laura, Sebastian, Michael, Monika, Joshi, Alex, Boris, Georgiana, Andra, … sorry if I missed someone!) who welcomed me in Uppsala and who made Swedish (winter) weather nicer and joyful!

A special thanks goes to my colleagues from the reflection seismology group (Bojan, George, Tatiana, Lea, Zibi, Myrto, Samuel, Mike, Kristina) who made every fieldwork memorable for me and who always gave an extra eye to my research. Thank you, guys and girls for being a such good friends, you are all amazing!

And last but not the least, I want to thank all senior researchers and professors within our program, especially Ayse, my co-supervisor and Chris, my initial co-supervisor, for supporting me all these years. And big thank you Maria for helping me with thesis summary translation!

Reza, thank you for helping me with deep-learning algorithms, it was a pleasure working with you and I hope we will have a chance to collaborate more in the future.

I was lucky to meet many friends outside of the workplace (Smart Exploration people, Musa and your super team, Javier, all the colleagues from Greece and many more of you from all sides of the Earth!) and I want to thank you all for being there for me and sharing unforgettable moments!

Big thanks to my family, both Serbian and Swedish. Without your support, everything would have been much harder. Nothing would be possible without you mom (Mimi). You are my wonder woman! You sacrificed these few years to come and take care of your grandkid, while your kid was doing PhD. THANK YOU MOM! Thank you, Luka, for your support at any time, you are the best brother (although you are the only brother).

I want to thank my friends in Serbia (Daca&Pile, Mina&Dragan, Draža, Miloš&Maja, Kaća, Anica, Kaća&Vejla, Pera, Đurica, Žaki, Jeka… I hope you won't be angry if I missed to write your names here, but know that you are always in my heart) for supporting me and welcoming me home, and always curious to hear about my adventures across the border.

Love, these acknowledgement pages are not enough to thank you. Above all, thank you for your love and being patient with me these years! Eloise, my sweetheart, I hope you will make your mom and dad proud. You are the highlight of my PhD studies, and I am so grateful to be your mother. You are amazing and your time is coming!

Magdalena Markovic,

Uppsala, September 2022

References

Adam. (1997). Seismic Exploration for VMS Deposits, Matagami, Québec.

Adam, E., Bohlen, T., & Milkereit, B. (2003a). Vertical Seismic Profiling at the Bell Allard Orebody, Matagami, Québec. Hardrock Seismic Exploration, 181–193. https://doi.org/10.1190/1.9781560802396.ch12

Adam, E., Perron, G., Arnold, G., Matthews, L., & Milkereit, B. (2003b). 3D Seismic Imaging for VMS Deposit Exploration, Matagami, Quebec. Hardrock Seismic Exploration, 229–246. https://doi.org/10.1190/1.9781560802396.CH15

AlBinHassan, N. M., & Marfurt, K. (2003). Fault detection using Hough transforms. SEG Technical Program Expanded Abstracts https://doi.org/10.1190/1.1817639

Allen, R. L., Lundström, I., Ripa, M., Simeonov, A., & Christofferson, H. (1996). Facies analysis of a 1.9 Ga, continental margin, back-arc, felsic caldera province with diverse Zn-Pb-Ag-(Cu-Au) sulfide and Fe oxide deposits, Bergslagen Region, Sweden. Economic Geology, 91(6), 979–1006. https://doi.org/10.2113/gsecongeo.91.6.979

Alofe, E. (2021). Reflection Seismic Survey for Characterising Historical Tailings and Deep Targeting at the Blötberget Mine, Central Sweden.

Balestrini, F., Draganov, D., Malehmir, A., Marsden, P., & Ghose, R. (2020). Improved target illumination at Ludvika mines of Sweden through seismic-interferometric surface-wave suppression. Geophysical Prospecting, 68, 200–213. https://doi.org/10.1111/1365-2478.12890

Bank, D., Koenigstein, N., & Giryes, R. (2020). Autoencoders. http://arxiv.org/abs/2003.05991

Bastani, M., & Joahansson, H. (2022). A New Data Acquisition System for Uav-Borne Vlf-Lf Measurements. Two Case Studies in Sweden. NSG2022 3rd Conference on Airborne, Drone and Robotic Geophysics https://doi.org/10.3997/2214-4609.202220068

Bauer, A., Walda, J., & Gajewski, D. (2022). Wavefield Decomposition for Diffraction Separation with a Convolutional Autoencoder for Seismic and Gpr Data. https://doi.org/10.3997/2214-4609.202210486

Bellefleur, G., Müller, C., Snyder, D., & Matthews, L. (2004). Downhole seismic imaging of a massive sulfide orebody with mode-converted waves, Halfmile lake, New Brunswick, Canada. Geophysics, 69(2), 318–329. https://doi.org/10.1190/1.1707051

Berkovitch, A., Belfer, I., Hassin, Y., & Landa, E. (2009). Diffraction imaging by multifocusing. Geophysics, 74(6), WCA75–WCA81. https://doi.org/10.1190/1.3198210

Birnie, C., Ravasi, M., Liu, S., & Alkhalifah, T. (2021). The potential of self-supervised networks for random noise suppression in seismic data. Artificial Intelligence in Geosciences, 2, 47–59. https://doi.org/10.1016/j.aiig.2021.11.001

Boschen, R. E., Rowden, A. A., Clark, M. R., & Gardner, J. P. A. (2013). Mining of deep-sea seafloor massive sulfides: A review of the deposits, their benthic communities, impacts from mining, regulatory frameworks and management strategies. Ocean & Coastal Management, 84, 54–67. https://doi.org/10.1016/j.ocecoaman.2013.07.005

Bräunig, L., Bräunig, B., Buske, S., Malehmir, A., Bäckström, E., Schön, M.& Marsden, P. (2020). Seismic depth imaging of iron-oxide deposits and their host rocks in the Ludvika mining area of central Sweden. Geophysical Prospecting, 68, 24–43. https://doi.org/10.1111/1365-2478.12836

Brodic, B., Malehmir, A., Juhlin, C., Dynesius, L., Bastani, M., & Palm, H. (2015). Multicomponent broadband digital-based seismic landstreamer for near-surface applications. Journal of Applied Geophysics, 123, 227–241. https://doi.org/10.1016/j.jappgeo.2015.10.009

Brodic, B., Malehmir, A., Pacheco, N., Juhlin, C., Carvalho, J., Dynesius, L., van den Berg, J., de Kunder, R., Donoso, G., Sjölund, T., & Araujo, V. (2021). Innovative seismic imaging of volcanogenic massive sulfide deposits, Neves-Corvo, Portugal - Part 1: In-mine array. Geophysics, 86(3), B165–B179. https://doi.org/10.1190/geo2020-0565.1

Budulan, G., McClenaghan, M. B., Layton-Matthews, D., Crabtree, D., Pyne, M., & McClenaghan, S. (2015). Indicator mineral signatures of the Halfmile Lake Zn-Pb-Cu volcanogenic massive sulphide deposit, Bathurst Mining Camp, New Brunswick: Part 1 - bedrock data. https://doi.org/10.4095/295586

Buntin, S., Malehmir, A., Koyi, H., Högdahl, K., Malinowski, M., Larsson, S. Å., Thybo, H., Juhlin, C., Korja, A., & Górszczyk, A. (2019). Emplacement and 3D geometry of crustal-scale saucer-shaped intrusions in the Fennoscandian Shield. Scientific Reports, 9(1), 1–11. https://doi.org/10.1038/s41598-019-46837-x

Calvert, A. J., Perron, G., & Li, Y. (2003). A Comparison of 2D Seismic Lines Shot over the Ansil and Bell Allard Mines in the Abitibi Greenstone Belt. Hardrock Seismic Exploration, 164–177. https://doi.org/10.1190/1.9781560802396.ch11

Campbell, G., & Crotty, J. H. (1990) 3D seismic mapping for mine planning purposes at the South Deep Prospect. Proceedings International Deep Mining Conference

Candès, E., Demanet, L., Donoho, D., & Ying, L. (2005). Fast Discrete Curvelet Transforms. http://www.curvelet.org

Candès, E. J., & Donoho, D. L. (2004). New tight frames of curvelets and optimal representations of objects with piecewise C2 singularities. Communications on Pure and Applied Mathematics, 57(2), 219–266. https://doi.org/10.1002/cpa.10116

Candès, E. J., & Guo, F. (2002). New multiscale transforms, minimum total variation synthesis: applications to edge-preserving image reconstruction. Signal Processing, 82(11), 1519–1543. https://doi.org/10.1016/S0165-1684(02)00300-6

Chen, L., Huo, S., & Shu, G. (2018). Seismic fault detection method based on Hough transform. 80th EAGE Conference and Exhibition: Opportunities Presented by the Energy Transition. https://doi.org/10.3997/2214-4609.201801268/cite/refworks

Cheraghi, S., Malehmir, A., & Bellefleur, G. (2012a). 3D imaging challenges in steeply dipping mining structures: New lights on acquisition geometry and processing from the Brunswick no. 6 seismic data, Canada. Geophysics, 77(5), WC109–WC122. https://doi.org/10.1190/geo2011-0475.1

da Col, F., Papadopoulou, M., Koivisto, E., Sito, Ł., Savolainen, M., & Socco, L. V. (2020). Application of surface-wave tomography to mineral exploration: a case study from Siilinjärvi, Finland. Geophysical Prospecting, 68(1), 254–269. https://doi.org/10.1111/1365-2478.12903

Debreil, J. A., Ross, P. S., & Mercier-Langevin, P. (2018). The Matagami District, Abitibi Greenstone Belt, Canada: Volcanic Controls on Archean Volcanogenic Massive Sulfide Deposits Associated with Voluminous Felsic Volcanism. Economic Geology, 113(4), 891–910. https://doi.org/10.5382/econgeo.2018.4575

Dehghannejad, M., Juhlin, C., Malehmir, A., Skyttä, P., & Weihed, P. (2010). Reflection seismic imaging of the upper crust in the Kristineberg mining area, northern Sweden. Journal of Applied Geophysics, 71(4), 125–136. https://doi.org/10.1016/j.jappgeo.2010.06.002

Dell, S., & Gajewski, D. (2011). Common-reflection-surface-based workflow for diffraction imaging. Geophysics, 76(5), S187–S195. https://doi.org/10.1190/geo2010-0229.1

Dell, S., Walda, J., Hoelker, A., & Gajewski, D. (2020). Categorizing and correlating diffractivity attributes with seismic-reflection attributes using autoencoder networks. Geophysics, 85(4), O59–O70. https://doi.org/10.1190/geo2019-0574.1/asset/images/large/figure11.jpeg

Ding, Y., & Malehmir, A. (2021). Reverse time migration (RTM) imaging of iron oxide deposits in the Ludvika mining area, Sweden. Solid Earth, 12(8), 1707–1718. https://doi.org/10.5194/se-12-1707-2021

Donoho, D. L., & Stark, P. B. (1989). Uncertainty Principles and Signal Recovery. SIAM Journal on Applied Mathematics, 49(3), 906–931. https://doi.org/10.1137/0149053

Donoso, G. A., Malehmir, A., Brodic, B., Pacheco, N., Carvalho, J., & Araujo, V. (2021). Innovative seismic imaging of volcanogenic massive sulfide deposits, Neves-Corvo, Portugal - Part 2: Surface array. Geophysics, 86(3), B181–B191. https://doi.org/10.1190/geo2020-0336.1/asset/images/large/figure9.jpeg

Dou, Q., Wei, L., Magee, D. R., & Cohn, A. G. (2017). Real-Time Hyperbola Recognition and Fitting in GPR Data. IEEE Transactions on Geoscience and Remote Sensing, 55(1), 51–62. https://doi.org/10.1109/tgrs.2016.2592679

Fomel, S. (2002). Applications of plane-wave destruction filters. Geophysics, 67(6), 1946–1960. https://doi.org/10.1190/1.1527095

Fomel, S., Landa, E., & Taner, M. T. (2007). Poststack velocity analysis by separation and imaging of seismic diffractions. Geophysics, 72(6), U89–U94. https://doi.org/10.1190/1.2781533

Galley, A. G., Hannington, M. D., & Jonasson, I. R. (2007). Mineral Deposits of Canada: A Synthesis of Major Deposit-Types, District Metallogeny, the Evolution of Geological Provinces, and Exploration Methods: Geological Association of Canada, Mineral Deposits Division. Special Publication, 5, 141–161.

Geng, Z., & Wang, Y. (2020). Physics-guided deep learning for predicting geological drilling risk of wellbore instability using seismic attributes data. Engineering Geology, 279, 105857. https://doi.org/10.1016/j.enggeo.2020.105857

Glaeser, A., Selvaraj, V., Lee, S., Hwang, Y., Lee, K., Lee, N., Lee, S., & Min, S. (2021). Applications of deep learning for fault detection in industrial cold forging. International Journal of Production Research, 59(16), 4826–4835. https://doi.org/10.1080/00207543.2021.1891318

Górszczyk, A., Adamczyk, A., & Malinowski, M. (2014). Application of curvelet denoising to 2D and 3D seismic data — Practical considerations. Journal of Applied Geophysics, 105, 78–94. https://doi.org/10.1016/j.jappgeo.2014.03.009

Heinonen, S., ImanñA, M., Snyder, D. B., Kukkonen, I. T., & Heikkinen, P. J. (2012). Seismic reflection profiling of the Pyhäsalmi VHMS-deposit: A complementary approach to the deep base metal exploration in Finland. Geophysics, 77(5), WC15–WC23. https://doi.org/10.1190/geo2011-0240.1

Heinonen, S., Malinowski, M., Hloušek, F., Gislason, G., Buske, S., Koivisto, E., & Wojdyla, M. (2019). Cost-effective seismic exploration: 2d reflection imaging at the kylylahti massive sulfide deposit, finland. Minerals, 9(5). https://doi.org/10.3390/min9050263

Hloušek, F., Malinowski, M., Bräunig, L., Buske, S., Malehmir, A., Markovic, M., Sito, L., Marsden, P., & Bäckström, E. (2022). Three-dimensional reflection seismic imaging of the iron oxide deposits in the Ludvika mining area, Sweden, using Fresnel volume migration. Solid Earth, 13(5), 917–934. https://doi.org/10.5194/se-13-917-2022

Jacquemin, P., & Mallet, J. L. (2005). Automatic Faults Extraction using double Hough Transform. SEG Technical Program Expanded Abstracts, 755–758. https://doi.org/10.1190/1.2144436

Jansson, N. F., & Allen, R. L. (2011). Timing of volcanism, hydrothermal alteration and ore formation at Garpenberg. Bergslagen, Sweden. GFF, 133, 1103–5897. https://doi.org/10.1080/11035897.2010.547597

Kaslilar, A., Wilczynski, Z., Markovic, M., Marsden, P., Manzi, M., & Malehmir, A. (2022). A Prefeasibility Study for Passive Seismic Imaging in Hard Rock Environment. https://doi.org/10.3997/2214-4609.202220166

Keller, J. B. (1962). Geometrical Theory of Diffraction, Journal of the Optical Society of America, 52(2), 116–130. https://doi.org/10.1364/josa.52.000116

Keydar, S., & Landa, E. (2019). Wave refocusing for linear diffractor using the time-reversal principle. Geophysical Prospecting, 67(5), 1345–1353. https://doi.org/10.1111/1365-2478.12784/cite/refworks

Klem-Musatov, K. (1994). Theory of Seismic Diffractions. https://doi.org/10.1190/1.9781560802617

Klem-Musatov, K. D., & Aizenberg, A. M. (1984). The ray method and the theory of edge waves. Undefined, 79(1), 35–50. https://doi.org/10.1111/j.1365-246x.1984.tb02839.x

Klokov, A., & Fomel, S. (2012). Separation and imaging of seismic diffractions using migrated dip-angle gathers. Geophysics, 77(6), S131–S143. https://doi.org/10.1190/geo2012-0017.1

Koivisto, E., Malehmir, A., Heikkinen, P., Heinonen, S., & Kukkonen, I. (2012). 2D reflection seismic investigations at the Kevitsa Ni-Cu-PGE deposit, northern Finland. Geophysics, 77(5), WC149–WC162. https://doi.org/10.1190/geo2011-0496.1

Kukkonen, I. T., Heinonen, S., Heikkinen, P., & Sorjonen-Ward, P. (2012). Delineating ophiolite-derived host rocks of massive sulfide Cu-Co-Zn deposits with 2D high-resolution seismic reflection data in Outokumpu, Finland. Geophysics, 77(5), WC213–WC222. https://doi.org/10.1190/geo2012-0029.1

Landa, E., & Keydar, S. (2012). Seismic monitoring of diffraction images for detection of local heterogeneities. Geophysics, 63(3), 1093–1100. https://doi.org/10.1190/1.1444387

Lin, P., Peng, S., Zhao, J., Cui, X., & Du, W. (2018). Accurate diffraction imaging for detecting small-scale geologic discontinuities. Geophysics, 83(5), S447–S457. https://doi.org/10.1190/geo2017-0545.1

Liu, S., Birnie, C., & Alkhalifah, T. (2022). Coherent noise suppression via a self-supervised blind-trace deep learning scheme. https://doi.org/10.48550/arxiv.2206.00301

Lowicki, F. (2017). Mineral resource estimate for the Blötberget iron ore project, Ludvika, Sweden, report by DMT Consulting Ltd.

Lowney, B., Lokmer, I., & O'Brien, G. S. (2021). Multi-domain diffraction identification: A supervised deep learning technique for seismic diffraction classification. Computers & Geosciences, 155, 104845. https://doi.org/10.1016/j.cageo.2021.104845

Magnusson, N. H. (1970). sveriges geologiska undersökning the origin of the iron ores in central sweden and the histor y of their alterations part I: text Stockholm.

Ma, H., Yin, D. Y., Liu, J. bin, & Chen, R. Z. (2022). 3D convolutional auto-encoder based multi-scale feature extraction for point cloud registration. Optics & Laser Technology, 149, 107860. https://doi.org/10.1016/j.optlastec.2022.107860

Malehmir, A. (2022). Ten Years of Mineral Exploration Innovation in Central Sweden. https://doi.org/10.3997/2214-4609.202220037

Malehmir, A., & Bellefleur, G. (2009). 3D seismic reflection imaging of volcanic-hosted massive sulfide deposits: Insights from reprocessing Halfmile Lake data, New Brunswick, Canada. Geophysics, 74(6), B209–B219. https://doi.org/10.1190/1.3230495

Malehmir, A., Dahlin, P., Lundberg, E., Juhlin, C., Sjöström, H., & Högdahl, K. (2011). Reflection seismic investigations in the Dannemora area, central Sweden: Insights into the geometry of polyphase deformation zones and magnetite-skarn deposits. Journal of Geophysical Research: Solid Earth, 116(11), 11307. https://doi.org/10.1029/2011jb008643

Malehmir, A., Durrheim, R., Bellefleur, G., Urosevic, M., Juhlin, C., White, D. J., Milkereit, B., & Campbell, G. (2012). Seismic methods in mineral exploration and mine planning: A general overview of past and present case histories and a look into the future. Geophysics, 77(5), WC173–WC190. https://doi.org/10.1190/geo2012-0028.1

Malehmir, A., Dynesius, L., Paulusson, K., Paulusson, A., Johansson, H., Bastani, M., Wedmark, M., & Marsden, P. (2017). The potential of rotary-wing UAV-based magnetic surveys for mineral exploration: A case study from central Sweden. Leading Edge, 36(7), 552–557. https://doi.org/10.1190/tle36070552.1

Malehmir, A., Gisselø, P., Socco, V. L., Carvalho, J., Marsden, P., Onar-Verboon, A., Loska, M., (2020). New ways of exploring subsurface with smart exploration solutions. First Break, 38(8), 77–89. https://doi.org/10.3997/1365-2397.fb20200f1

Malehmir, A., Juhlin, C., Wijns, C., Urosevic, M., Valasti, P., & Koivisto, E. (2012). 3D reflection seismic imaging for open-pit mine planning and deep exploration in the Kevitsa Ni-Cu-PGE deposit, northern Finland. Geophysics, 77(5), WC95–WC108. https://doi.org/10.1190/geo2011-0468.1

Malehmir, A., Koivisto, E., Manzi, M., Cheraghi, S., Durrheim, R. J., Bellefleur, G., Wijns, C., Hein, K. A. A., & King, N. (2014). A review of reflection seismic investigations in three major metallogenic regions: The Kevitsa Ni–Cu–PGE district (Finland), Witwatersrand goldfields (South Africa), and the Bathurst Mining Camp (Canada). Ore Geology Reviews, 56, 423–441. https://doi.org/10.1016/j.oregeorev.2013.01.003

Malehmir, A., Maries, G., Bäckström, E., Schön, M., & Marsden, P. (2017). Developing cost-effective seismic mineral exploration methods using a landstreamer and a drophammer. Scientific Reports, 7(1). https://doi.org/10.1038/s41598-017-10451-6

Malehmir, A., Markovic, M., Marsden, P., Gil, A., Buske, S., Sito, L., Bäckström, E., Sadeghi, M., & Luth, S. (2021). Sparse 3D reflection seismic survey for deep-targeting iron oxide deposits and their host rocks, Ludvika Mines, Sweden. Solid Earth, 12(2), 483–502. https://doi.org/10.5194/se-12-483-2021

Malehmir, A., Tryggvason, A., Juhlin, C., Rodriguez-Tablante, J., & Weihed, P. (2006). Seismic imaging and potential field modelling to delineate structures hosting VHMS deposits in the Skellefte Ore District, northern Sweden. Tectonophysics, 426(3–4), 319–334. https://doi.org/10.1016/j.tecto.2006.08.006

Ma, M., Zhang, R., & Ajo-Franklin, J. (2020). A workflow of separating and imaging diffraction wave by using deep learning network: An application of GPR data. SEG Technical Program Expanded Abstracts, 2020-October, 1920–1924. https://doi.org/10.1190/segam2020-3427448.1

Manzi, M. S. D., Cooper, G. R. J., Malehmir, A., & Durrheim, R. J. (2020). Improved structural interpretation of legacy 3D seismic data from Karee platinum mine (South Africa) through the application of novel seismic attributes. Geophysical Prospecting, 68(1), 145–163. https://doi.org/10.1111/1365-2478.12900

Manzi, M. S. D., Gibson, M. A. S., Hein, K. A. A., King, N., & Durrheim, R. J. (2012). Application of 3D seismic techniques to evaluate ore resources in the West Wits Line goldfield and portions of the West Rand goldfield, South Africa. Geophysics, 77(5), WC163–WC171. https://doi.org/10.1190/geo2012-0133.1

Maries, G., Malehmir, A., Bäckström, E., Schön, M., & Marsden, P. (2017). Downhole physical property logging for iron-oxide exploration, rock quality, and mining: An example from central Sweden. Ore Geology Reviews, 90, 1–13. https://doi.org/10.1016/j.oregeorev.2017.10.012

Maries, G., Malehmir, A., & Marsden, P. (2020). Cross-profile seismic data acquisition, imaging, and modeling of iron-oxide deposits: A case study from Blötberget, south-central Sweden. Geophysics, 85(6), B233–B247. https://doi.org/10.1190/geo2020-0173.1

Markovic, M., Malehmir, R., & Malehmir, A. (2022a). Diffraction pattern recognition using deep semantic segmentation. Near Surface Geophysics, 20(5), 507-518. https://doi.org/10.1002/nsg.12227

Markovic, M., Maries, G., Malehmir, A., von Ketelhodt, J., Bäckström, E., Schön, M., & Marsden, P. (2020). Deep reflection seismic imaging of iron-oxide deposits in the Ludvika mining area of central Sweden. Geophysical Prospecting, 68(1), 7–23. https://doi.org/10.1111/1365-2478.12855

Matthews, L. (2002). Base metal exploration: Looking deeper and adding value with seismic data: CSEG Recorder.

Milkereit, B., Berrer, E. K., King, A. R., Watts, A. H., Roberts, B., Adam, E., Eaton, D. W., Wu, J., & Salisbury, M. H. (2012). Development of 3-D seismic exploration technology for deep nickel-copper deposits—A case history from the Sudbury basin, Canada. Geophysics, 65(6), 1890–1899. https://doi.org/10.1190/1.1444873

Milkereit, B., Eaton, D., & Berrer, E. (1996). Towards 3-D seismic exploration technology for the crystalline crust. SEG Annual Meeting, 638–641. https://doi.org/10.1190/1.1826727

Milkereit, B., Eaton, D., Wu, J., Perron, G., Salisbury, M., Berrer, E. K., & Morrison, G. (1996). Seismic imaging of massive sulfide deposits: part II. Reflection seismic profiling. Economic Geology, 91(5), 829–834. https://doi.org/10.2113/gsecongeo.91.5.829

Naghizadeh, M., & Sacchi, M. (2018). Ground-roll attenuation using curvelet downscaling. Geophysics, 83(3), V185–V195. https://doi.org/10.1190/geo2017-0562.1

Neelamani, R., Baumstein, A. I., Gillard, D. G., Hadidi, M. T., & Soroka, W. L. (2008). Coherent and random noise attenuation using the curvelet transform. Leading Edge (Tulsa, OK), 27(2), 240–248. https://doi.org/10.1190/1.2840373

Orozco-Del-Castillo, M. G., Ortiz-Alemán, C., Martin, R., Ávila-Carrera, R., & Rodríguez-Castellanos, A. (2011). Seismic data interpretation using the Hough transform and principal component analysis. Journal of Geophysics and Engineering, 8(1), 61–73. https://doi.org/10.1088/1742-2132/8/1/008

Papadopoulou, M., da Col, F., Mi, B., Bäckström, E., Marsden, P., Brodic, B., Malehmir, A., & Socco, L. V. (2020). Surface-wave analysis for static corrections in mineral exploration: A case study from central Sweden. Geophysical Prospecting, 68, 214–231. https://doi.org/10.1111/1365-2478.12895

Pertuz, T., Malehmir, A., Bos, J., Brodic, B., Ding, Y., de Kunder, R., & Marsden, P. (2022). Broadband seismic source data acquisition and processing to delineate iron oxide deposits in the Blötberget mine-central Sweden. Geophysical Prospecting, 70, 79–94. https://doi.org/10.1111/1365-2478.13159

Place, J., Malehmir, A., Högdahl, K., Juhlin, C., & Nilsson, K. P. (2015). Seismic characterization of the Grängesberg iron deposit and its mining-induced structures, central Sweden. Interpretation, 3(3), SY41–SY56. https://doi.org/10.1190/int-2014-0212.1

Puzyrev, V., Salles, T., Surma, G., & Elders, C. (2022). Geophysical model generation with generative adversarial networks. Geoscience Letters, 9(1), 1–9. https://doi.org/10.1186/s40562-022-00241-y

Ripa, M. (2001). Economic geology research and documentation, Volume 2 2001–2002.

Roberts, B., Zaleski, E., Perron, G., Adam, E., Petrie, L., & Salisbury, M. (2003). Seismic Exploration of the Manitouwadge Greenstone Belt, Ontario: A Case History. Hardrock Seismic Exploration, 110–126. https://doi.org/10.1190/1.9781560802396.ch7

Rochlin, I., Landa, E., & Keydar, S. (2021). Detection of subsurface lineaments using edge diffraction. Geophysics, 86(3), WA99–WA107. https://doi.org/10.1190/geo2020-0367.1

Ronneberger, O., Fischer, P., & Brox, T. (2015). U-net: Convolutional networks for biomedical image segmentation. Lecture Notes in Computer Science (Including Subseries Lecture Notes in Artificial Intelligence and Lecture Notes in Bioinformatics), 9351, 234–241. https://doi.org/10.1007/978-3-319-24574-4_28/cover

Saad, O. M., & Chen, Y. (2020). Deep denoising autoencoder for seismic random noise attenuation. Geophysics, 85(4), V367–V376. https://doi.org/10.1190/geo2019-0468.1

Schwarz, B. (2019). Coherent wavefield subtraction for diffraction separation. Geophysics, 84(3), V157–V168. https://doi.org/10.1190/geo2018-0368.1

Schwarz, B., & Krawczyk, C. M. (2020). Coherent diffraction imaging for enhanced fault and fracture network characterization. Solid Earth, 11(5), 1891–1907. https://doi.org/10.5194/se-11-1891-2020

Singh, B., Malinowski, M., Górszczyk, A., Malehmir, A., Buske, S., Sito, L., & Marsden, P. (2022). 3D high-resolution seismic imaging of the iron oxide deposits in Ludvika (Sweden) using full-waveform inversion and reverse time migration. Solid Earth, 13(6), 1065–1085. https://doi.org/10.5194/se-13-1065-2022

Staal, C. R. van, Wilson, R. A., Rogers, N., Fyffe, L. R., Langton, J. P., McCutcheon, S. R., McNicoll, V., & Ravenhurst, C. E. (2003). Geology and Tectonic History of the Bathurst Supergroup, Bathurst Mining Camp, and Its Relationships to Coeval Rocks in Southwestern New Brunswick and Adjacent Maine—A Synthesis. Massive Sulfide Deposits of the Bathurst Mining Camp, New Brunswick, and Northern Maine. https://doi.org/10.5382/mono.11.03

Starck, J. L., Candès, E. J., & Donoho, D. L. (2002). The curvelet transform for image denoising. IEEE Transactions on Image Processing, 11(6), 670–684. https://doi.org/10.1109/tip.2002.1014998

Stephens, M. B., Ripa M., Lundstrom I., Persson L., Bergman T. (2009). Synthesis of the Bedrock Geology in the Bergslagen Region, Fennoscandian Shield, South-Central Sweden. Sveriges geologiska undersokning

Tschannen, V., Ettrich, N., Delescluse, M., & Keuper, J. (2020). Detection of point scatterers using diffraction imaging and deep learning. Geophysical Prospecting, 68, 830–844. https://doi.org/10.1111/1365-2478.12889

Urosevic, M., Bhat, G., & Grochau, M. H. (2013). Targeting nickel sulfide deposits from 3D seismic reflection data at Kambalda, Australia. Geophysics, 77(5), WC123–WC132. https://doi.org/10.1190/geo2011-0514.1

Urosevic, M., Stolz, E., Kepic, A., & Juhlin, C. (2007). Seismic exploration of ore deposits in Western Australia. Decennial Mineral Exploration Conferences.

Vermeer, G. J. O. (2010). 3D symmetric sampling of sparse acquisition geometries. Geophysics, 75(6), WB3–WB14. https://doi.org/10.1190/1.3496903

von Ketelhodt, J. K., Manzi, M. S. D., & Durrheim, R. J. (2019). Post-stack denoising of legacy reflection seismic data: implications for coalbed methane exploration, Kalahari Karoo Basin, Botswana. Exploration Geophysics, 50(6), 667–682. https://doi.org/10.1080/08123985.2019.1660576

Wang, Z., & AlRegib, G. (2014). Automatic fault surface detection by using 3D hough transform. SEG Technical Program Expanded Abstracts. https://doi.org/10.1190/segam2014-1590.1

Zhu, Z., Wang, X., Bai, S., Yao, C., & Bai, X. (2014). Deep Learning Representation using Autoencoder for 3D Shape Retrieval. Neurocomputing, 204, 41–50. https://doi.org/10.48550/arxiv.1409.7164

Acta Universitatis Upsaliensis

Digital Comprehensive Summaries of Uppsala Dissertations from the Faculty of Science and Technology 2195

Editor: The Dean of the Faculty of Science and Technology

A doctoral dissertation from the Faculty of Science and Technology, Uppsala University, is usually a summary of a number of papers. A few copies of the complete dissertation are kept at major Swedish research libraries, while the summary alone is distributed internationally through the series Digital Comprehensive Summaries of Uppsala Dissertations from the Faculty of Science and Technology. (Prior to January, 2005, the series was published under the title "Comprehensive Summaries of Uppsala Dissertations from the Faculty of Science and Technology".)

Distribution: publications.uu.se
urn:nbn:se:uu:diva-481754

ACTA
UNIVERSITATIS
UPSALIENSIS
UPPSALA
2022